



OPEN ACCESS

EDITED BY

Geoffrey Robert Mitchell,
Polytechnic Institute of Leiria, Portugal

REVIEWED BY

Amir R. Masoodi,
Ferdowsi University of Mashhad, Iran
Chitaranjan Pany,
Vikram Sarabhai Space Centre, India

*CORRESPONDENCE

Zhenyu Zhou,
✉ zzy660909@126.com

RECEIVED 28 March 2025

ACCEPTED 03 July 2025

PUBLISHED 30 July 2025

CITATION

Zhou Z (2025) Differential quadrature free vibration analysis of sandwich plates with curvilinear fiber variable stiffness composite face sheets.

Front. Mater. 12:1601813.

doi: 10.3389/fmats.2025.1601813

COPYRIGHT

© 2025 Zhou. This is an open-access article distributed under the terms of the [Creative Commons Attribution License \(CC BY\)](https://creativecommons.org/licenses/by/4.0/). The use, distribution or reproduction in other forums is permitted, provided the original author(s) and the copyright owner(s) are credited and that the original publication in this journal is cited, in accordance with accepted academic practice. No use, distribution or reproduction is permitted which does not comply with these terms.

Differential quadrature free vibration analysis of sandwich plates with curvilinear fiber variable stiffness composite face sheets

Zhenyu Zhou*

College of Aerospace Engineering, Nanjing University of Aeronautics and Astronautics, Nanjing, China

Free vibration calculations of Sandwich plates with curvilinear fiber variable stiffness composite face sheets usually require a significant computing effort to obtain a high computational accuracy. An improved approach integrating the differential quadrature method (DQM) and first-order shear deformation theory (FSDT) is introduced in this work. The skins of sandwich plates are composed of one or several layers of variable stiffness composite laminates (VSCL) with fiber paths assumed to follow a specific linear pattern. The FSDT and von Kármán strain–displacement relationship were used to derive the governing equations of the sandwich plate, and DQM was applied to discretize such governing equations and solve for the fundamental frequency of the sandwich plate. The computational results were verified and compared with other FSDT–based computational results, and there was good agreement with the suggested model. Also, the variation patterns of the natural frequency under different parameters such as fiber orientation angles, boundary conditions, number of layers, and core/skin thickness were investigated. The novelty of this study lies in the first application of an integrated DQM-FSDT approach to the free vibration analysis of sandwich plates with variable-stiffness curvilinear fiber composites. Notably, this method attains accuracy comparable to higher-order models (<5% error) with merely a 19×19 mesh. Key results demonstrate that optimizing the fiber path can enhance the fundamental frequency of VSCL sandwich plates by up to 32.7% (CFFF boundary), providing an efficient design tool for vibration control of aerospace lightweight structures.

KEYWORDS

free vibration, sandwich plate, variable stiffness composite laminates, curvilinear fibers, differential quadrature method

1 Introduction

The high stiffness-to-weight ratio property of VSCL sandwich plates holds significant promise for their application in lightweight structures, such as aircraft wings, satellite fairings, and wind turbine blades. Typically, a sandwich construction has three sections: a top, middle, and bottom segment with a core located in the center and skins at the top and bottom (Vinson, 1999), where the skins have the same material and thickness while the core can be made of almost any material or architecture. The face sheets require

high strength (Carrera and Brischetto, 2009) and the core requires light weight. Noor et al. (1996) first systematically demonstrated that sandwich plates have very high stiffness-to-weight ratio and strength-to-weight ratio properties, and Noor et al. (1996) further verified the advantages of the mechanical properties of sandwich plates through computational modelling. Based on these properties, sandwich plates are widely used in aerospace, automotive and other engineering applications (Siriruk et al., 2009). Langdon et al. (2012) specifically investigated the blast resistance of sandwich plates in marine structures. Osa-uwagboe et al. (2023), on the other hand, explored the innovative application of sandwich plates in large structures such as wind turbine blades. Sandwich structures offer significant advantages, such as high strength-to-weight ratios. These benefits, coupled with ongoing discoveries of new materials (Vinson, 2001), drive their continued use in structural design. The conventional skins of constant stiffness composite laminates (CSCL) consist of straight fibers whose stiffness, such as elasticity and flexibility, remains uniform or constant in all directions in the plane of the material. While VSCL are typically made by carefully designing and arranging layers of different materials or by altering the path of reinforcing fibers (curvilinear fiber) in the construction. Advanced technologies (e.g., automated layup) enable curved fiber placement by controlling fiber orientation. This results in continuous variation of fiber angles, as illustrated in Figure 1. As a result, the variable stiffness composite plate and shell with curvilinear fiber can be fabricated, as shown in Figure 2. (Yaman and Önal, 2016) It is obvious that a more flexible method of increasing a plate's rigidity can be achieved by using VSCL. (Setoodeh et al., 2009) Researchers (Akhavan and Ribeiro, 2018) have recently used theoretical analysis, empirical and semi-empirical modelling, numerical simulations, and experimental testing to examine the mechanical properties of sandwich constructions. Experimental data is typically used to verify the modelling, (Yazdani and Ribeiro, 2015), while numerical simulations (Antunes et al., 2020) are preferred for their computational efficiency and rapid turnaround time.

The foundation for VSCL has been laid by numerous academics using the statics analysis of CSCL sandwich plates. Kant and Swaminathan. (2001) have analyzed the fundamental frequency of CSCL laminates and sandwich plates and the solution method used is finite element. They used a higher-order refined theory as the basis for their modelling and as parametric inputs, they systematically changed the plate thickness, the ratio of core to skin thickness, and the boundary conditions. Furthermore, their investigation included a rigorous comparative analysis with established methods to demonstrate the precision and robustness of their chosen theory. Yuan and Dawe. (2002) looked at the vibration properties of conventional sandwich plates that are rectangular in shape, including the natural frequencies and modes, using the spline finite strip method and it was concluded that the techniques of single-plate analysis were not applicable to the structural analysis of most plate structures. To lower the computational cost in the fundamental frequency prediction of sandwich plates and composite laminates, Mantari and Ore. (2015) presented a simplified FSDT. Reducing the amount of unknowns in the modelling computations allows for the reduction of the number of degrees of freedom. Comparing the computational results with those of other computational models serves as verification of the method's accuracy. Rezaiee-Pajand and

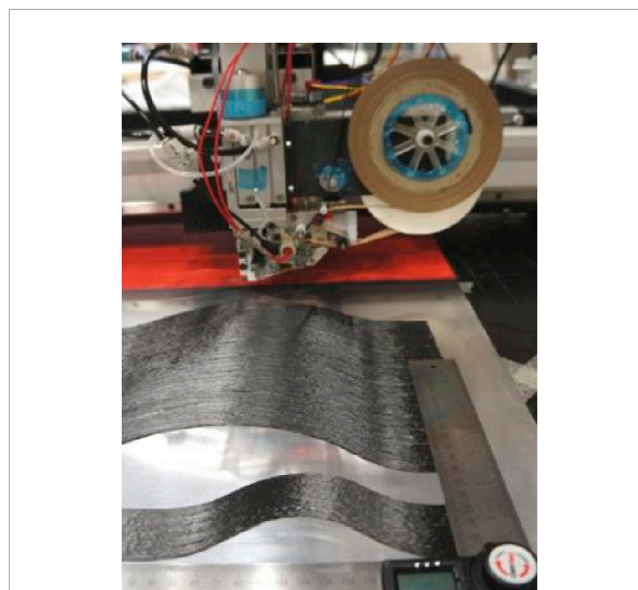


FIGURE 1
Automatic wire laying machine and curved fiber layers.

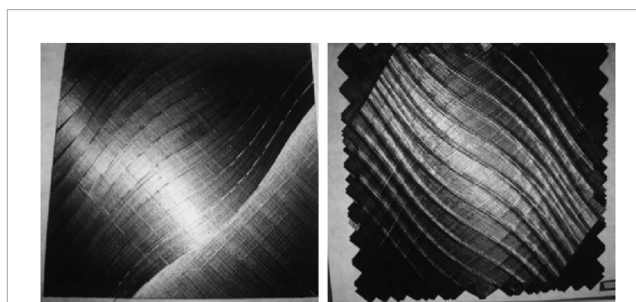


FIGURE 2
Variable stiffness composite plates.

Masoodi. (2019) developed a mixed-interpolated triangular shell element using MITC theory and total Lagrangian formulation, effectively mitigating shear/membrane locking in buckling/post-buckling analysis of plates/shells, with novel benchmarks validating accuracy for complex curved structures.

The advent of advanced technologies ushered in a new era of VSCL plates and revolutionized the design landscape of composite plates. By manipulating the fiber orientation, VSCL plates offer improved mechanical properties by altering the stiffness distribution. Gürdal and Olmedo, (1993) used a numerical model to solve static problems such as displacement field and overall stiffness of VSCL symmetric laminates. They pointed out that by choosing an appropriate starting and ending angle, the given loading conditions can be better considered and a certain stiffness can be achieved or possibly the buckling behavior can be improved. Lopes et al. (2008) predicted various failure modes of VSCL plates in compression and simulated the first layer failure in post-buckling. Finite element modelling was used to predict the physical failure criteria for different modes of failure of the VSCL plates. Khani et al. (2011) applied a new solution to incorporate the failure

criteria for strength into the parameter space of the laminates. The numerical results showed an increase in strength compared with the quasi-isotropic construction. Akhavan and Ribeiro. (2011) analyzed the law of variation of fundamental frequencies and mode shapes with fiber orientation angles for VSCL laminates, third-order shear deformation theory (TSDT) was the modelling technique applied, and p -version finite elements were employed in the solution. Through data comparison, they explored some connections that exist between fiber orientation angles and fundamental frequencies.

Existing research on VSCL plates focuses on statics and has only investigated their dynamics to a limited extent, which warrants further research into their dynamics in future studies. Houmat. (2020) and Hachemi. (2020); Hachemi. (2022) are among the few scholars who have performed free vibration analysis of VSCL sandwich plates. The modelling theory used by Houmat is three-dimensional elasticity theory, while the analysis of Hachemi is grounded in both layer-wise theory and HSDT. They both chose p -version finite elements as the solution method. By adjusting factors including fiber orientation angles, boundary conditions, and skin-to-core thickness ratios, the variation patterns of fundamental frequencies as well as other dynamic responses were examined, highlighting the benefits of VSCL sandwich plates in structural investigations.

Systems of partial differential equations that typically have difficult-to-find closed-form solutions characterize engineering challenges. (Civalek, 2008) Consequently, engineers and researchers frequently turn to approximative numerical techniques to solve such systems. These methods include the finite element, the p -version finite element, the Rayleigh–Ritz methods, the finite volume method and so on. Pany. (2022) developed a PS-FEM model using triangular shell elements to estimate wave propagation constants in line-supported periodic plates, enabling efficient prediction of bandgap characteristics and multi-span panel frequencies through propagation surface discretization. Pany and Li. (2023) combined periodic structure theory with FEM to model wave propagation in metamaterials and pressurized frames, enabling non-reciprocal transmission and prestress simulation. Bellman and Casti. (1971) developed the differential quadrature technique (DQM) for solving partial differential equations. DQM has the advantage of having a smaller number of discrete points with higher computational accuracy. Liu. (2001) utilized Mindlin plate theory as the modelling theory and applied DQM to the investigation of rectangular plate buckling. Liew et al. (1996) used DQM to conduct a static study of a rectangular plate on Winkler's basis, utilizing FSDT as the modelling theory. This is the first successful application of DQM to thick-plate problems. Based on previous work, Liew et al. (2003) applied the moving least squares differential quadrature (MLSDQ) to calculate and study the fundamental frequency of symmetric laminates of medium thickness and the modelling theory is FSDT. The free vibration problem of sandwich plates with functional grades on an elastic foundation was investigated by Fu et al. (2020). They employed DQM, and the modelling theory is NSDT. Ghandehari et al. (2025) modeled temp-dependent CNT-reinforced nested conical shells via FSDT/GDQM, introducing elastic interlayers and arbitrary BCs for vibration analysis under thermal loads. Mottaghi et al. (2025) employed FSDT and Hamilton's principle for modelling and GDQM for solving, investigating the free vibration of CNT-reinforced polymer composite rings,

analyzing agglomeration, porosity, and elastic coupling effects. Innovatively, they developed a novel CBR model, unraveling multifactor coupling mechanisms. To the best of our knowledge, no studies have yet applied the DQM to the free vibration analysis of VSCL sandwich plates modelling by FSDT.

This work proposes an FSDT-based DQM approach to give a reasonably accurate and computationally cheap computer model for the free vibration analysis of VSCL sandwich structures. The plate consists of two VSCL skins and an isotropic core. Based on the FSDT, the governing equations were derived using the von Kármán strain–displacement relationship and Hamilton's principle. By applying the DQM, the fundamental frequencies of the sandwich plates were determined numerically, and the impacts of several parameters on the plate's vibration behaviour were examined. Distinguishing from existing studies that mostly use the finite element method to analyze VSCL structures, this study is the first to apply the combination of DQM and FSDT to the free vibration analysis of VSCL sandwich plates with curvilinear fiber. The method significantly reduces the computational cost by reducing the number of grid points (only 19×19 grids are required) while maintaining comparable accuracy to higher-order models (see Tables 2, 3), providing a new way for efficient dynamic modelling under complex boundary conditions.

This is how the remainder of the paper is structured. The modelling procedure and analytical method employed are stated in the second section. In the third section, numerical applications and discussion, encompassing both CSCL and VSCL sandwich plates, are presented. The last section summarizes the conclusions.

2 Theoretical formulation

2.1 Geometric description

The geometrical design and parameterization of a sandwich plate with variable stiffness skins are displayed in Figure 3. The upper and lower composite skins, every stratum of the skin consisting of single or laminated composite layers with curvilinear fibers, with a soft core in the centre, make up the entire plate, assume that the dimensions of the plate are a , b , and h , respectively, for length, breadth, and thickness. The total thickness h can be decomposed into upper and lower skins h_s and intermediate core h_c . It is considered that every interface on the board is flawlessly integrated. Given that the entire plate consists of N layers, the thickness of each single layer of the face sheet is $h_{layer} = 2h_s/(N - 1)$. The entire plate's Cartesian coordinate system is specified as $0 \leq X \leq a, 0 \leq Y \leq b, -h/2 \leq Z \leq h/2$.

To simplify the definition, the point of central symmetry of the reference path is typically specified to be at the center of each individual layer of the skin, as illustrated in Figure 3, and the Cartesian coordinate system is defined as $-a/2 \leq x \leq a/2, -b/2 \leq x \leq b/2, -h_{layer}/2 \leq z \leq h_{layer}/2$. Assuming that the angle of the fiber direction varies linearly along the x -direction, it is expressed mathematically in Equation 1: (Akhavan and Ribeiro, 2011):

$$\begin{cases} \theta(x) = \frac{2(\Theta_1 - \Theta_0)}{a}|x| + \Theta_0 \\ y' = \frac{dy}{dx} = \tan \theta(x) \end{cases} \quad (1)$$

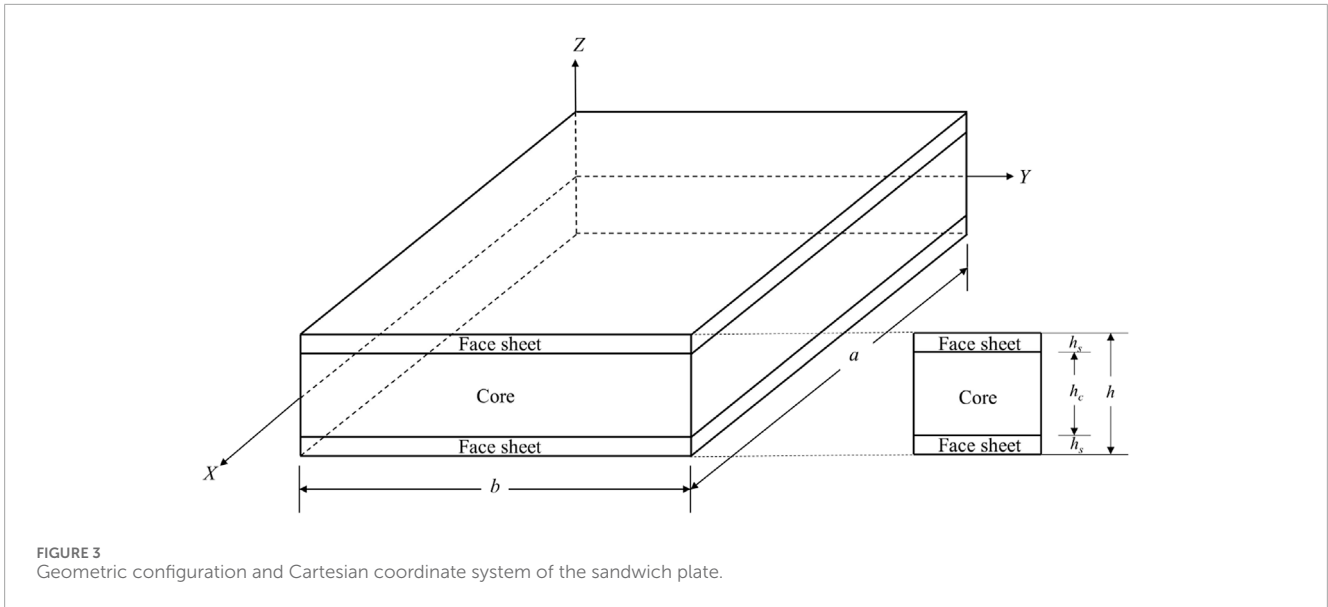


FIGURE 3 Geometric configuration and Cartesian coordinate system of the sandwich plate.

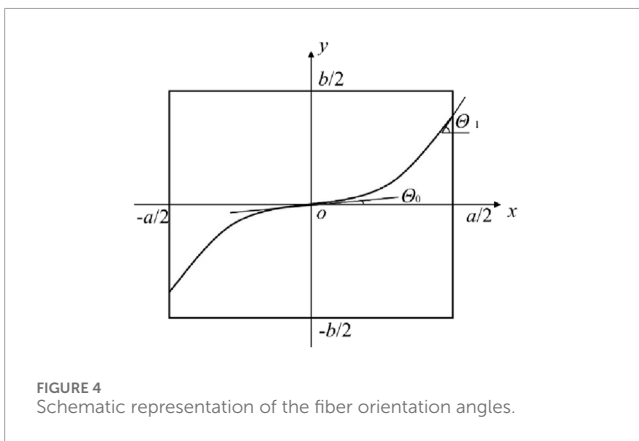


FIGURE 4 Schematic representation of the fiber orientation angles.

where, Θ_0 is the starting angle of the fiber, characterizing the angle between the tangent of the fiber curve at the center point and the x -axis of the relative horizontal line, the fiber's ending angle, or Θ_1 , is the angle formed by the tangent of the fiber curve and the x -axis of the relative horizontal line at the location where the layer's outer boundary is $a/2$, and a is the plate length. Figure 4 shows the schematic diagram of the the fiber orientation angles.

Integrating the above equation gives the reference path for the curvilinear fiber placement as Equation 2:

$$y(x) = \begin{cases} \frac{a}{2(\Theta_1 - \Theta_0)} \left\{ \ln(\cos \Theta_0) - \ln \left[\cos \left(\frac{2(\Theta_1 - \Theta_0)}{a} x + \Theta_0 \right) \right] \right\} & (0 \leq x \leq \frac{a}{2}) \\ \frac{a}{2(\Theta_0 - \Theta_1)} \left\{ \ln(\cos \Theta_0) - \ln \left[\cos \left(\frac{2(\Theta_0 - \Theta_1)}{a} x + \Theta_0 \right) \right] \right\} & (-\frac{a}{2} \leq x \leq 0) \end{cases} \quad (2)$$

2.2 Modelling theory

Between the skin and core materials of sandwich plates, there are significant differences in stiffness and material properties,

making the performance analysis of the sandwich structure quite intricate. As a result, the calculation model selected has a significant impact on how accurately the sandwich structure is calculated. (Pandey and Pradyumna, 2015). Transverse shear deformation is not taken into account by the classical laminated plate theory (CLPT), which is predicated on Kirchhoff's assumptions. Therefore, for plates of moderate thickness, CLPT's estimates on both static and dynamic analysis are biased. (Abrate, 2008; Zare et al., 2015; Pushparaj and Suresha, 2016; Belarbi et al., 2017). For the purpose of this study's free vibration analysis of sandwich plates, the author employed the FSDT modelling theory, (Reddy, 2004), which accounts for the impact of shear deformation.

In this study, the FSDT theory and the linear part of the von Kármán strain-displacement relationship [the nonlinear term is neglected in Equation 4] are used, which is suitable for the linear analysis of free vibration under small deformations. Based on the first two assumptions of Kirchhoff (the normal remains straight and perpendicular to the midplane), this study ignores the third assumption (ignoring the positive strain in the thickness direction), and adopts the FSDT theory to consider the transverse shear deformation. In case a symmetric sandwich plate is used, the vibrations in the transverse and in-plane directions are separated by the symmetry in the z direction, and the in-plane deformation at $z=0$ can be ignored. The displacement field has the following expression as Equation 3 (Mindlin, 1951).

$$\begin{aligned} u(x, y, z, t) &= u_0(x, y, t) + z\varphi_x(x, y, t) \\ v(x, y, z, t) &= v_0(x, y, t) + z\varphi_y(x, y, t) \\ w(x, y, z, t) &= w_0(x, y, t) \end{aligned} \quad (3)$$

where the displacements along the three coordinate axes are denoted by u , v , and w , and the midplane of the plate rotates about the x and y axes at angles φ_x and φ_y , respectively.

Per the von Kármán strain-displacement relationship, linear strain components are:

$$\begin{Bmatrix} \varepsilon_x \\ \varepsilon_y \\ \gamma_{yz} \\ \gamma_{xz} \\ \gamma_{xy} \end{Bmatrix} = \begin{Bmatrix} \frac{\partial u_0}{\partial x} + \frac{1}{2} \left(\frac{\partial w_0}{\partial x} \right)^2 \\ \frac{\partial v_0}{\partial y} + \frac{1}{2} \left(\frac{\partial v_0}{\partial y} \right)^2 \\ \frac{\partial w_0}{\partial y} + \varphi^y \\ \frac{\partial w_0}{\partial x} + \varphi^x \\ \frac{\partial u_0}{\partial y} + \frac{\partial v_0}{\partial x} + \frac{\partial w_0}{\partial x} \frac{\partial w_0}{\partial y} \end{Bmatrix} + z \begin{Bmatrix} \frac{\partial \varphi^x}{\partial x} \\ \frac{\partial \varphi^y}{\partial y} \\ 0 \\ 0 \\ \frac{\partial \varphi^x}{\partial y} + \frac{\partial \varphi^y}{\partial x} \end{Bmatrix} \quad (4)$$

Applying Hooke's law and assuming plane stress, the stress components of the plate areas are obtained in the following way:

$$\begin{Bmatrix} \sigma_x \\ \sigma_y \\ \tau_{xy} \\ \tau_{xz} \\ \tau_{yz} \end{Bmatrix} = \begin{bmatrix} \bar{Q}_{11} & \bar{Q}_{12} & \bar{Q}_{16} & 0 & 0 \\ \bar{Q}_{12} & \bar{Q}_{22} & \bar{Q}_{62} & 0 & 0 \\ \bar{Q}_{61} & \bar{Q}_{26} & \bar{Q}_{66} & 0 & 0 \\ 0 & 0 & 0 & \bar{Q}_{55} & \bar{Q}_{54} \\ 0 & 0 & 0 & \bar{Q}_{45} & \bar{Q}_{44} \end{bmatrix} \begin{Bmatrix} \varepsilon_x \\ \varepsilon_y \\ \gamma_{xy} \\ \gamma_{xz} \\ \gamma_{yz} \end{Bmatrix} \quad (5)$$

where \bar{Q}_{ij} are given in the following way:

$$\begin{aligned} [\bar{Q}] &= \begin{bmatrix} \bar{Q}_{11} & \bar{Q}_{12} & \bar{Q}_{16} \\ \bar{Q}_{21} & \bar{Q}_{22} & \bar{Q}_{62} \\ \bar{Q}_{61} & \bar{Q}_{26} & \bar{Q}_{66} \end{bmatrix} = [T_\sigma] \begin{bmatrix} Q_{11} & Q_{12} & 0 \\ Q_{21} & Q_{22} & 0 \\ 0 & 0 & Q_{66} \end{bmatrix} [T_\sigma]^T \\ [\bar{Q}_s] &= \begin{bmatrix} \bar{Q}_{55} & \bar{Q}_{54} \\ \bar{Q}_{45} & \bar{Q}_{44} \end{bmatrix} = [T_s] \begin{bmatrix} Q_{55} & 0 \\ 0 & Q_{44} \end{bmatrix} [T_s]^T \\ [T_\sigma] &= \begin{bmatrix} \cos^2 \theta & \sin^2 \theta & -2 \sin \theta \cos \theta \\ \sin^2 \theta & \cos^2 \theta & 2 \sin \theta \cos \theta \\ \sin \theta \cos \theta & -\sin \theta \cos \theta & \cos^2 \theta - \sin^2 \theta \end{bmatrix} \\ [T_s] &= \begin{bmatrix} \cos \theta & \sin \theta \\ -\sin \theta & \cos \theta \end{bmatrix} \end{aligned} \quad (6)$$

where

$$\begin{aligned} Q_{11} &= \frac{E_1}{1 - \nu_{12}\nu_{21}}, Q_{22} = \frac{E_2}{1 - \nu_{12}\nu_{21}}, Q_{12} = \frac{\nu_{21}E_1}{1 - \nu_{12}\nu_{21}}, \\ Q_{66} &= G_{12}, Q_{55} = kG_{13}, Q_{44} = kG_{23} \end{aligned} \quad (7)$$

where E_i , G_{ij} , and ν_{ij} are the mechanical properties and $k = 5/6$ is the shear correction factor used in this study. The shear correction factor $k = 5/6$ is derived from the Reissner energy consistency criterion (Birman and Bert, 2002), applicable under the assumption of a quadratic distribution of transverse shear stresses for homogeneous or symmetric sandwich cross-sections.

Hamilton's principle can be used to generate the moving equations in the following way: (Reddy, 2004):

$$\int_{t_1}^{t_2} \delta(U - T) dt = 0 \quad (8)$$

where U is the strain form and T is the kinetic form of energy, respectively.

The strain energy can be shown in the following way:

$$U = \iiint_V \frac{1}{2} (\sigma_x \varepsilon_x + \sigma_y \varepsilon_y + \sigma_z \varepsilon_z + \tau_{xy} \gamma_{xy} + \sigma_{yz} \gamma_{yz} + \tau_{xz} \gamma_{xz}) dV \quad (9)$$

The kinetic energy can be shown in the following way:

$$T = \iiint_V \frac{1}{2} \rho(z) \left[\left(\frac{\partial u}{\partial t} \right)^2 + \left(\frac{\partial v}{\partial t} \right)^2 + \left(\frac{\partial w}{\partial t} \right)^2 \right] dV \quad (10)$$

The moving equations for the sandwich plate's free vibration may be acquired by substituting Equations 4,-7,9,10 into Equation 8:

$$\begin{cases} \frac{\partial Q_x}{\partial x} + \frac{\partial Q_y}{\partial y} = I_0 \frac{\partial^2 w}{\partial t^2} \\ \frac{\partial M_x}{\partial x} + \frac{\partial M_{xy}}{\partial y} - Q_x = I_2 \frac{\partial^2 \varphi_x}{\partial t^2} \\ \frac{\partial M_y}{\partial y} + \frac{\partial M_{xy}}{\partial x} - Q_y = I_2 \frac{\partial^2 \varphi_y}{\partial t^2} \end{cases}, \quad (11)$$

where $I_i = \int_{-\frac{h}{2}}^{\frac{h}{2}} \rho z^i dz, i = 0, 2,$

2.3 Equation of motion

The stress resultants M_{ij} and transverse shear force Q_{ij} can be determined by integrating the stresses in each single layer along the direction of thickness.

$$\begin{aligned} \begin{Bmatrix} M_x \\ M_y \\ M_{xy} \end{Bmatrix} &= \int_{-\frac{h}{2}}^{\frac{h}{2}} z \begin{Bmatrix} \sigma_x \\ \sigma_y \\ \tau_{xy} \end{Bmatrix} dz = \begin{bmatrix} D_{11} & D_{12} & D_{16} \\ D_{12} & D_{22} & D_{26} \\ D_{16} & D_{26} & D_{66} \end{bmatrix} \begin{Bmatrix} \frac{\partial \varphi_x}{\partial x} \\ \frac{\partial \varphi_y}{\partial y} \\ \frac{\partial \varphi_x}{\partial y} + \frac{\partial \varphi_y}{\partial x} \end{Bmatrix}, \\ \begin{Bmatrix} Q_y \\ Q_x \end{Bmatrix} &= \int_{-\frac{h}{2}}^{\frac{h}{2}} \begin{Bmatrix} \tau_{yz} \\ \tau_{xz} \end{Bmatrix} dz = \begin{bmatrix} A_{44} & A_{45} \\ A_{45} & A_{55} \end{bmatrix} \begin{Bmatrix} \varphi_y + \frac{\partial w}{\partial y} \\ \varphi_x + \frac{\partial w}{\partial x} \end{Bmatrix}, \end{aligned} \quad (12)$$

Equation 11 can be substituted with Equation 12 to assemble the following formulations for the governing equations of the sandwich plate's free vibration.

$$A_{55} \left(\frac{\partial \varphi_x}{\partial x} + \frac{\partial^2 w}{\partial x^2} \right) + A_{45} \left(\frac{\partial \varphi_y}{\partial x} + \frac{\partial \varphi_x}{\partial y} + 2 \frac{\partial^2 w}{\partial x \partial y} \right) + A_{44} \left(\frac{\partial \varphi_y}{\partial y} + \frac{\partial^2 w}{\partial y^2} \right) = I_0 \frac{\partial^2 w}{\partial t^2}, \quad (13)$$

$$\begin{aligned} D_{11} \frac{\partial^2 \varphi_x}{\partial x^2} + D_{12} \frac{\partial^2 \varphi_y}{\partial x \partial y} + D_{16} \left(2 \frac{\partial^2 \varphi_x}{\partial x \partial y} + \frac{\partial^2 \varphi_y}{\partial x^2} \right) + D_{26} \frac{\partial^2 \varphi_y}{\partial y^2} + D_{66} \left(\frac{\partial^2 \varphi_x}{\partial y^2} + \frac{\partial^2 \varphi_y}{\partial x \partial y} \right) \\ - A_{55} \left(\varphi_x + \frac{\partial w}{\partial x} \right) - A_{45} \left(\varphi_y + \frac{\partial w}{\partial y} \right) = I_2 \frac{\partial^2 \varphi_x}{\partial t^2}, \end{aligned} \quad (14)$$

$$\begin{aligned} D_{16} \frac{\partial^2 \varphi_x}{\partial x^2} + D_{66} \left(\frac{\partial^2 \varphi_x}{\partial x \partial y} + \frac{\partial^2 \varphi_y}{\partial x^2} \right) + D_{12} \frac{\partial^2 \varphi_x}{\partial x \partial y} + D_{22} \frac{\partial^2 \varphi_y}{\partial y^2} + D_{26} \left(\frac{\partial^2 \varphi_x}{\partial y^2} + 2 \frac{\partial^2 \varphi_y}{\partial x \partial y} \right) \\ - A_{45} \left(\varphi_x + \frac{\partial w}{\partial x} \right) - A_{44} \left(\varphi_y + \frac{\partial w}{\partial y} \right) = I_2 \frac{\partial^2 \varphi_y}{\partial t^2} \end{aligned} \quad (15)$$

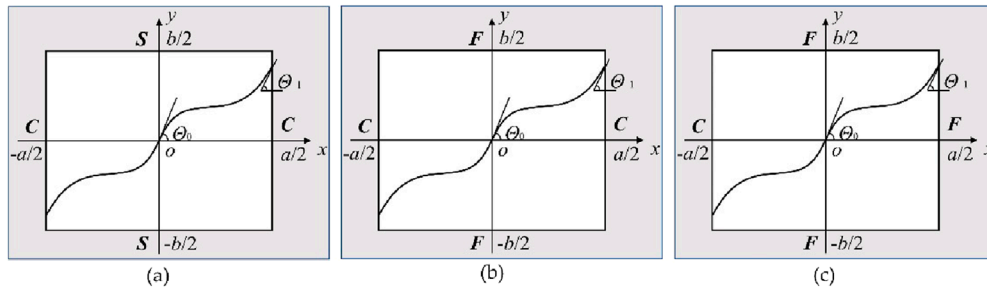


FIGURE 5 Definition of boundary conditions for sandwich plates: (a) CSCS; (b) CFCF; (c) CFFF.

where A_{ij} and D_{ij} are the stretching and bending stiffnesses, respectively, and the expressions are given in Equation 16.

$$A_{ij} = \sum_{k=1}^n (\bar{Q}_{ij})_k (z_k - z_{k-1}) \tag{16}$$

$$D_{ij} = \frac{1}{3} \sum_{k=1}^n (\bar{Q}_{ij})_k (z_k^3 - z_{k-1}^3)$$

A_{ij} are stiffness coefficients related to internal forces and midplane strains only, collectively referred to as stretching stiffness. D_{ij} are stiffness coefficients related to internal moments with respect to curvature and twist rate, collectively referred to as bending stiffness.

2.4 Differential quadrature method

DQM is essentially a differential equation in the function at each node of the derivative with the calculation of the region of all nodes at the function value of the weighted sum to replace. (Bellman and Casti, 1971). The required differential equation’s numerical solution can be found in the resultant system of equations. This is how DQM transforms the differential equation solution problem into the linear equation system solving problem. (Shu et al., 2002; 2004; Thai et al., 2014; Malikan and Far, 2018). Supplementary Appendix SI provides the specific implementation of this technique.

To simplify the calculation, for the DQM discretization of the moving equations, the expressions for the weighting coefficients were obtained:

$$\bar{A}_{ij}^{(1)} = \frac{A_{ij}^{(1)}}{a}, \bar{B}_{ij}^{(1)} = \frac{B_{ij}^{(1)}}{b}, \bar{A}_{ij}^{(2)} = \frac{A_{ij}^{(2)}}{a^2}, \bar{B}_{ij}^{(2)} = \frac{B_{ij}^{(2)}}{b^2} \tag{17}$$

The separating variables for the displacement terms (w , φ^x , and φ^y) can be written in the following way:

$$w(x, y, t) = W(x, y)e^{i\omega t}, \varphi_x(x, y, t) = \psi_x(x, y)e^{i\omega t}, \varphi_y(x, y, t) = \psi_y(x, y)e^{i\omega t} \tag{18}$$

where $W(x, y)$ is the vibration mode function, φ_x and φ_y are the rotational angles functions and ω is the fundamental frequency of the sandwich plate.

To facilitate subsequent calculations and comparisons, the data are dimensionless as follows:

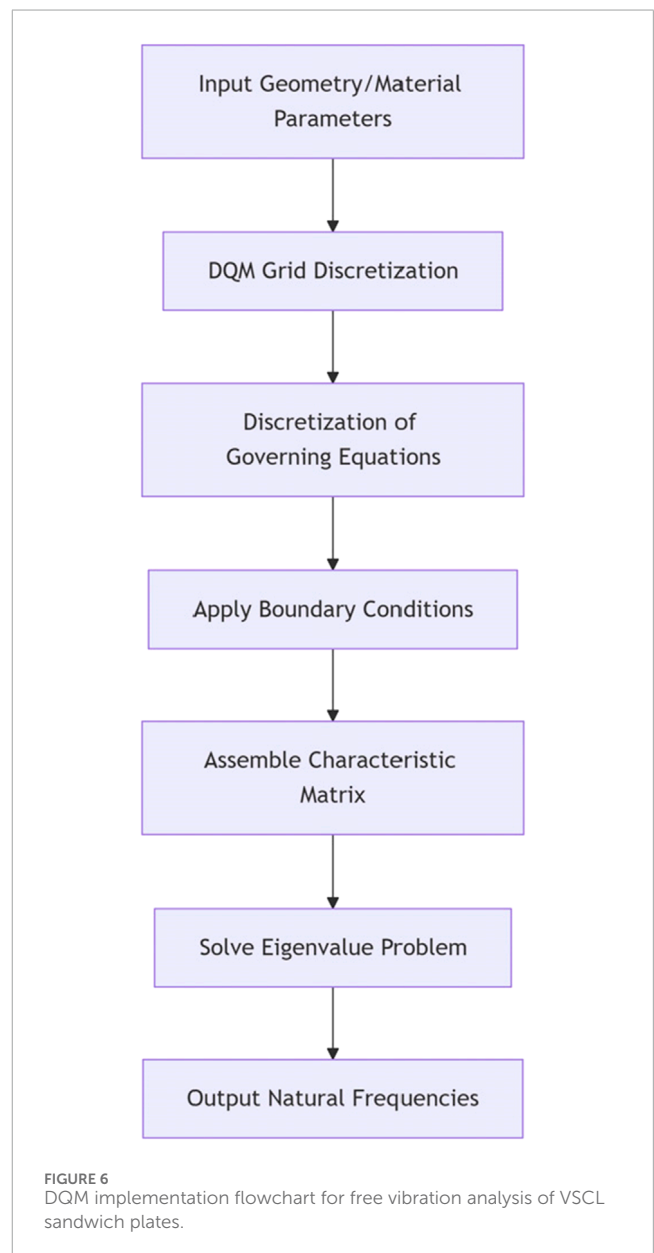


FIGURE 6 DQM implementation flowchart for free vibration analysis of VSCL sandwich plates.

TABLE 1 Mechanical properties of the materials.

	Material ID	Material name	E_1 (GPa)	E_2 (GPa)	G_{12} (GPa)	G_{13} (GPa)	G_{23} (GPa)	ν_{12}	ρ (kg/m ³)
Face sheets	I	Carbon/Epoxy	131	10.34	6.895	6.205	6.895	0.22	1,627
	II	Carbon/Epoxy	138	8.96	7.1	7.1	7.1	0.30	1800
Core	III	Polyurethane foam	6.89×10^{-3}	6.89×10^{-3}	3.45×10^{-3}	3.45×10^{-3}	3.45×10^{-3}	0.30	97
	IV	PVC foam	0.04	0.04	0.016	0.016	0.06	0.25	100
	V	Balsa wood	0.104	0.104	0.05	0.05	0.05	0.32	130
	VI	Aluminum honeycomb	0.057	0.328	0.056	1.115	2.2×10^{-3}	0.406	335.762

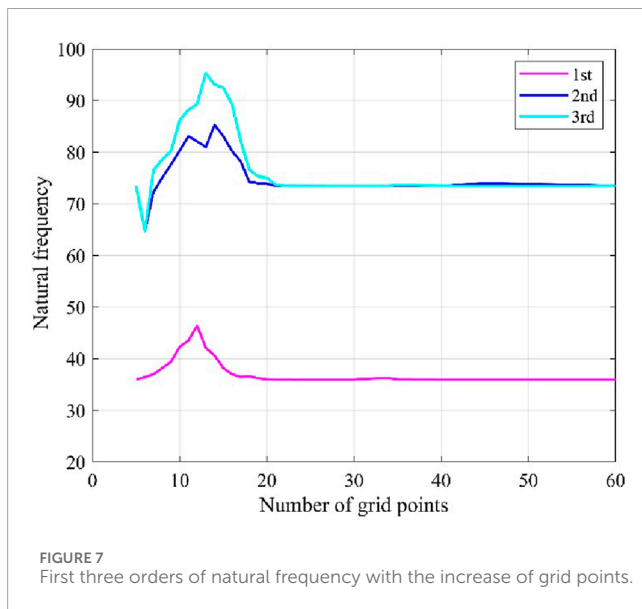


FIGURE 7 First three orders of natural frequency with the increase of grid points.

$$\xi = \frac{x}{a}, \eta = \frac{y}{b}, D_{ij}(\xi) = \frac{[D]}{D_{110}}, A_{ij}(\xi) = \frac{[A]}{A_{440}}, \bar{\omega} = \frac{\omega b^2}{h} \sqrt{\left(\frac{\rho}{E_2}\right)} \quad (19)$$

where D_{110} represents $D_{11}(x)$ at $x = 0$ and A_{440} represents $A_{44}(x)$ at $x = 0$.

Substituting Equations 17–19 into Equations 13–15 and performing a DQM discretization, the governing equations can be shown as follows:

$$\begin{aligned} & A_{55}(\xi_i) \sum_{m=1}^{N_x} \bar{A}_{im}^{(2)} W_{mj} + A_{44}(\xi_i) \sum_{n=1}^{N_y} \bar{B}_{jn}^{(2)} W_{in} + 2A_{45}(\xi_i) \sum_{m=1}^{N_x} \bar{A}_{im}^{(1)} \sum_{n=1}^{N_y} \bar{B}_{jn}^{(1)} W_{mn} \\ & + A_{55}(\xi_i) \sum_{m=1}^{N_x} \bar{A}_{im}^{(1)} \psi_{x,mj} + A_{45}(\xi_i) \sum_{n=1}^{N_y} \bar{B}_{jn}^{(1)} \psi_{x,in} + A_{45}(\xi_i) \sum_{m=1}^{N_x} \bar{A}_{im}^{(1)} \psi_{y,mj} \\ & + A_{44}(\xi_i) \sum_{n=1}^{N_y} \bar{B}_{jn}^{(1)} \psi_{y,in} = -I_0 \bar{\omega}^2 W_{ij} \end{aligned} \quad (20)$$

$$\begin{aligned} & - A_{55}(\xi_i) \sum_{m=1}^{N_x} \bar{A}_{im}^{(1)} W_{mj} - A_{45}(\xi_i) \sum_{m=1}^{N_x} \bar{B}_{jn}^{(1)} W_{in} - A_{55}(\xi_i) \psi_{x,mn} \\ & + D_{11}(\xi_i) \sum_{m=1}^{N_x} \bar{A}_{im}^{(2)} \psi_{x,mj} + 2D_{16}(\xi_i) \sum_{m=1}^{N_x} \bar{A}_{im}^{(1)} \sum_{n=1}^{N_y} \bar{B}_{jn}^{(1)} \psi_{x,mn} + D_{66}(\xi_i) \sum_{n=1}^{N_y} \bar{B}_{jn}^{(2)} \psi_{x,in} \\ & - A_{45}(\xi_i) \psi_{y,mn} + D_{16}(\xi_i) \sum_{m=1}^{N_x} \bar{A}_{im}^{(2)} \psi_{y,mj} + D_{26}(\xi_i) \sum_{n=1}^{N_y} \bar{B}_{jn}^{(2)} \psi_{y,in} \\ & + (D_{12}(\xi_i) + D_{66}(\xi_i)) \sum_{m=1}^{N_x} \bar{A}_{im}^{(1)} \sum_{n=1}^{N_y} \bar{B}_{jn}^{(1)} \psi_{y,mn} = -I_2 \bar{\omega}^2 \psi_{x,ij} \end{aligned} \quad (21)$$

$$\begin{aligned} & - A_{45}(\xi_i) \sum_{m=1}^{N_x} \bar{A}_{im}^{(1)} W_{mj} - A_{44}(\xi_i) \sum_{m=1}^{N_x} \bar{B}_{jn}^{(1)} W_{in} \\ & - A_{45}(\xi_i) \psi_{x,mn} + D_{16}(\xi_i) \sum_{m=1}^{N_x} \bar{A}_{im}^{(2)} \psi_{x,mj} + D_{26}(\xi_i) \sum_{n=1}^{N_y} \bar{B}_{jn}^{(2)} \psi_{x,in} \\ & + (D_{66}(\xi_i) + D_{12}(\xi_i)) \sum_{m=1}^{N_x} \bar{A}_{im}^{(1)} \sum_{n=1}^{N_y} \bar{B}_{jn}^{(1)} \psi_{x,mn} \\ & - A_{44}(\xi_i) \psi_{y,mn} + D_{66}(\xi_i) \sum_{m=1}^{N_x} \bar{A}_{im}^{(2)} \psi_{y,mj} + D_{22}(\xi_i) \sum_{n=1}^{N_y} \bar{B}_{jn}^{(2)} \psi_{y,in} \\ & + 2D_{26}(\xi_i) \sum_{m=1}^{N_x} \bar{A}_{im}^{(1)} \sum_{n=1}^{N_y} \bar{B}_{jn}^{(1)} \psi_{y,mn} = -I_2 \bar{\omega}^2 \psi_{y,ij} \end{aligned} \quad (22)$$

where

$$W_{ij} = W(\xi_i, \eta_j), \psi_{x,ij} = \psi_x(\xi_i, \eta_j), \psi_{y,ij} = \psi_y(\xi_i, \eta_j) \quad (23)$$

To simplify the calculation, Equations 20–22 can be stated more succinctly as Equations 24 or 25:

$$\begin{bmatrix} K_{1,W} & K_{1,\psi^x} & K_{1,\psi^y} \\ K_{2,W} & K_{2,\psi^x} & K_{2,\psi^y} \\ K_{3,W} & K_{3,\psi^x} & K_{3,\psi^y} \end{bmatrix} \begin{Bmatrix} W \\ \psi^x \\ \psi^y \end{Bmatrix} = -\bar{\omega}^2 \begin{bmatrix} I_0 & 0 & 0 \\ 0 & I_2 & 0 \\ 0 & 0 & I_2 \end{bmatrix} \begin{Bmatrix} W \\ \psi^x \\ \psi^y \end{Bmatrix} \quad (24)$$

or

$$[K]\{R\} = -\bar{\omega}^2 [I]\{R\}, \{R\} = \{\{W\}^T \{\psi^x\}^T \{\psi^y\}^T\}^T \quad (25)$$

Similarly, the boundary conditions can be derived by discretization using the DQM

$$\{T\}\{R\} = \{0\} \quad (26)$$

The solution of the specific matrix $\{T\}$ is given in the next section.

TABLE 2 The dimensionless fundamental frequency of anti-symmetric [0/90/core/0/90] sandwich plate ($a/b = 1, t_c/t_f = 10$).

a/h	Methods			
	Ref(Kant and Swaminathan, 2001)	Ref (Mantari and Ore, 2015)	Ref (Whitney and Pagano, 1970)	Present
2	5.2017	5.6114	5.6114	5.3246
4	9.0312	9.5447	9.5447	9.2547
10	13.8694	14.1454	14.1454	14.2559
20	15.5295	15.6124	15.6124	15.6742
30	15.9155	15.9438	15.9438	15.8596
40	16.0577	16.0655	16.0655	16.0028
50	16.1264	16.1229	16.1229	16.1256
60	16.1612	16.1544	16.1544	16.1698
70	16.1845	16.1735	16.1735	16.1752
80	16.1991	16.1859	16.1859	16.1872
90	16.2077	16.1944	16.1944	16.1966
100	16.2175	16.2006	16.2006	16.2369

TABLE 3 The dimensionless fundamental frequency of anti-symmetric [0/90/core/0/90] sandwich plate ($t_c/t_f = 10, a/h = 10$).

a/b	Methods			
	Ref (Kant and Swaminathan, 2001)	Ref (Mantari and Ore, 2015)	Ref (Whitney and Pagano, 1970)	Present
0.5	39.4840	40.3559	40.1511	40.2645
1	13.8694	14.1454	14.1454	14.2559
1.5	9.4910	9.8376	9.7826	9.3789
2	10.1655	8.0759	7.9863	8.1679
2.5	6.5059	6.9340	6.8463	6.9473
3	5.6588	6.0727	5.9993	6.0227
5	3.6841	3.9929	3.9658	4.0763

To find the basic frequencies, or eigenvalues, and the accompanying eigenvectors, all mesh points were divided into two groups: internal domain points and boundary points. The boundary points, indicated by $\{b\}$ in vector form, are situated at the plate's four edges. The domain points are the set of all remaining interior points and are denoted by $\{d\}$. Boundary conditions are substituted into the governing equations. The resulting system is then divided and rearranged into the following matrix equation:

$$\begin{bmatrix} K_{bb} & K_{bd} \\ K_{db} & K_{dd} \end{bmatrix} \begin{Bmatrix} R_b \\ R_d \end{Bmatrix} = -\bar{\omega}^2 \begin{Bmatrix} 0 \\ R_d \end{Bmatrix} \tag{27}$$

By eliminating the non-zero element $\{R_b\}$, Equation 27 can be shown in the following way:

$$(\bar{K} - \bar{\omega}^2)\{R_d\} = 0 \tag{28}$$

where $\bar{K} = K_{dd} - K_{db}K_{bb}^{-1}K_{bd}$. The fundamental frequencies and amplitudes of the plate can be determined by solving Equation (28) using the standard eigenvalue matrix.

2.5 Boundary conditions

This study covers five types of boundary conditions: four-side clamped support (CCCC), four-side simply support (SSSS),

TABLE 4 Comparative study of the first four orders of the natural frequency of the VSCL plate.

[$\langle \theta_0, \theta_1 \rangle$]	Boundary conditions	Method	Mode			
			1	2	3	4
[$\langle 0, 52 \rangle$]	CCCC	Present	68.428	132.785	134.836	206.419
		Hachemi (2020)	70.759	134.180	135.917	207.917
		Hachemi et al. (2020)	70.76	134.180	135.920	207.920
[$\langle 0, 50 \rangle$]	SSSS	Present	42.587	95.179	96.274	158.179
		Hachemi (2020)	45.259	96.156	98.511	159.112
		Hachemi et al. (2020)	45.260	96.160	98.510	159.110
[$\langle 0, 35 \rangle$]	SFFC	Present	7.923	28.571	70.576	71.891
		Hachemi (2020)	8.144	29.578	71.339	72.236
		Hachemi et al. (2020)	8.140	29.580	71.270	72.230
[$\langle 0, 45 \rangle$]	FCSC	Present	43.271	71.025	120.852	124.932
		Hachemi (2020)	44.931	71.638	121.091	125.784
		Hachemi et al. (2020)	44.930	71.640	121.090	125.780

The difference between the results and the reference stems from the fact that the reference used layer-wise theory (LWT) to accurately describe the deformation in the thickness direction, whereas the present study used FSDT to simplify the model, resulting in a deviation of $\leq 4.8\%$ in the calculation of the higher-order modes.

TABLE 5 First and second natural frequencies of the VSCL sandwich square plate [$\pm(\theta_0|\theta_1)_s/core/\pm(\theta_0|\theta_1)_s$], material II and material IV, CCCC.

Mode	θ_0	θ_1					
		0	10	30	50	70	90
1	0	6.9527	6.9507	6.9469	6.9353	6.9234	6.9187
	10	6.9567	6.9714	6.9709	6.9563	6.9507	6.9457
	30	7.0264	7.0402	7.0410	7.0154	6.9912	6.9542
	50	9.3974	7.1262	7.1094	7.0565	7.0051	6.9721
	70	7.1675	7.1753	7.1462	7.0852	7.0095	6.9871
	90	7.0478	7.0756	7.0947	7.0678	7.0145	6.9923
	2	0	8.9047	8.9219	8.9851	9.0576	9.1216
10		8.9209	8.9581	9.0495	9.1234	9.1876	9.2137
30		9.0898	9.1422	9.2457	9.3088	9.2852	9.2943
50		9.3519	9.4053	9.4747	9.3883	9.2260	9.2127
70		9.5884	9.6095	9.4978	9.2751	9.0877	9.0622
90		9.9746	9.9823	9.9946	9.8496	9.0347	9.0014

TABLE 6 First and second natural frequencies of the VSCL sandwich square plate [$\pm(\theta_0|\theta_1)_s/core/\pm(\theta_0|\theta_1)_s$], material II and material IV, SSSS.

Mode	θ_0	θ_1					
		0	10	30	50	70	90
1	0	6.3067	6.3409	6.4822	6.5774	6.5977	6.6124
	10	6.3272	6.3885	6.5296	6.6102	6.6269	6.6314
	30	6.4312	6.5006	6.6158	6.6561	6.6488	6.6572
	50	6.5537	6.5946	6.6688	6.6735	6.6101	6.6016
	70	6.5528	6.5856	6.6296	6.6106	6.5174	6.4174
	90	6.4736	6.5469	6.6026	6.5863	6.4936	6.4247
	2	0	8.3372	8.3594	8.4891	8.6027	8.6967
10		8.3577	8.4062	8.5464	8.6607	8.7622	8.8451
30		8.5293	8.601	8.7364	8.8492	8.8618	8.8924
50		8.7891	8.8465	8.9353	8.9003	8.7389	8.7137
70		8.9093	8.9362	8.8803	8.7339	8.5645	8.4547
90		9.3178	9.3267	9.3756	9.3149	8.9146	8.8472

TABLE 7 First and second natural frequencies of the VSCL sandwich square plate $[\pm(\Theta_0|\Theta_1)_s/core/\pm(\Theta_0|\Theta_1)_s]$, material II and material VI, CCCC.

Mode	Θ_0	Θ_1					
		0	10	30	50	70	90
1	0	11.0793	11.0781	11.0697	11.0648	11.0453	11.0357
	10	11.0771	11.0953	11.0914	11.0766	11.0756	11.0714
	30	11.1549	11.1668	11.1625	11.1398	11.1157	11.1047
	50	13.5267	11.2479	11.2376	11.1803	11.1316	11.1243
	70	11.2943	11.1749	11.3022	11.2033	11.2733	11.3478
	90	11.2223	11.2055	11.1914	11.1375	11.1398	11.2047
	2	0	36.0282	36.0495	36.1104	36.1777	36.2433
10		36.0492	36.0856	36.1773	36.2468	36.3136	36.3224
30		36.2157	36.266	36.3757	36.4304	36.4078	36.3924
50		36.4774	36.5317	36.5965	36.5162	36.3525	36.2176
70		36.7176	37.0954	36.7352	37.1054	36.6247	36.7341
90		37.1175	36.3956	36.9743	36.2134	36.1622	36.1527

TABLE 8 First and second natural frequencies of the VSCL sandwich square plate $[\pm(\Theta_0|\Theta_1)_s/core/\pm(\Theta_0|\Theta_1)_s]$, material II and material VI, SSSS.

Mode	Θ_0	Θ_1					
		0	10	30	50	70	90
1	0	10.4352	10.4633	10.6112	10.7011	10.7187	10.7231
	10	10.4534	10.5097	10.6595	10.7313	10.7482	10.7513
	30	10.5547	10.6224	10.7407	10.7839	10.7782	10.7924
	50	10.6788	10.7174	10.7937	10.7974	10.7397	10.8043
	70	10.6768	10.7098	10.7523	10.7334	10.6432	10.6243
	90	10.5944	10.6674	10.7316	10.7103	10.6142	10.5378
	2	0	35.4595	35.4859	35.6165	35.7305	35.8212
10		35.4812	35.5335	35.6683	35.7815	35.8853	35.9136
30		35.6575	35.7275	35.8633	35.9785	35.9869	36.0034
50		35.9093	35.9717	36.0571	36.0281	35.8644	35.9436
70		36.0297	36.0617	36.0074	35.8588	35.6927	35.6219
90		36.4395	36.4497	36.5019	36.4393	36.0425	35.9547

TABLE 9 The first two natural frequencies of the VSCL sandwich square plate $[(\Theta_0|\Theta_1)/core/(\Theta_0|\Theta_1)]$, CCCC.

Mode	Θ_0	Θ_1			
		0	30	50	70
1	0	39.6473	39.6247	39.6030	39.5948
	30	39.6313	39.3563	39.3423	39.3246
	50	39.5363	39.3478	39.2798	39.2636
	70	39.6216	39.5347	39.4298	39.4889
2	0	58.9473	59.7766	60.8274	61.2839
	30	58.8647	59.5879	59.3649	59.3278
	50	58.8897	59.8846	59.8808	59.2867
	70	58.9146	59.9078	59.2678	59.2475

Bold indicates straight fiber layups with equal starting and ending angles.

TABLE 10 The first two natural frequencies of the VSCL sandwich square plate $[(\Theta_0|\Theta_1)/core/(\Theta_0|\Theta_1)]$, SSSS.

Mode	Θ_0	Θ_1			
		0	30	50	70
1	0	34.2142	35.0553	35.9351	35.1028
	30	34.1379	35.6275	35.9874	35.1498
	50	34.2378	35.4367	36.0994	35.7698
	70	34.5134	35.4793	35.8569	34.9646
2	0	54.0617	55.2244	56.8894	58.1559
	30	54.0024	56.2285	56.9712	57.1236
	50	54.3478	56.4783	57.0087	56.2863
	70	54.7369	56.8923	55.8963	55.1944

Bold indicates straight fiber layups with equal starting and ending angles.

opposite-side clamped support-simply support (CSCS), opposite-side clamped support-free (CFCF), and three-side clamped support-free on one side (CFFF), whose mathematical expressions are presented in Equations 29–31. Figure 5 illustrates the constraint schematics of CSCS, CFCF and CFFF.

The following are the boundary condition phrases for each edge.

(a) Clamped (C)

$$w = \varphi^x = \varphi^y = 0, x = 0 \text{ or } x = 1 (y = 0 \text{ or } y = 1), \quad (29)$$

(b) Simply supported (S)

TABLE 11 The first two natural frequencies of the VSCL sandwich square plate $[(\Theta_0|\Theta_1)/core/(\Theta_0|\Theta_1)]$, CSCS.

Mode	Θ_0	Θ_1			
		0	30	50	70
1	0	37.5031	37.8185	38.4084	37.9751
	30	37.4231	37.3931	37.3647	37.2168
	50	37.3895	37.3678	37.3476	37.1678
	70	37.2336	37.1436	37.0247	36.8877
2	0	57.8964	58.7024	60.1376	58.7718
	30	57.6423	58.3142	59.1235	57.9871
	50	57.1278	58.1756	57.8934	57.9923
	70	56.5671	56.2726	56.3179	56.1968

Bold indicates straight fiber layups with equal starting and ending angles.

TABLE 13 The first two natural frequencies of the VSCL sandwich square plate $[(\Theta_0|\Theta_1)/core/(\Theta_0|\Theta_1)]$, CFFF.

Mode	Θ_0	Θ_1			
		0	30	50	70
1	0	8.5298	8.7551	9.4121	11.3263
	30	9.1572	9.2474	10.0278	11.5621
	50	10.5317	10.6781	10.8187	12.4623
	70	12.2578	12.6712	12.9152	13.2824
2	0	16.6078	17.0308	17.8546	19.3829
	30	17.8254	18.3633	18.9512	19.4782
	50	18.2756	18.4278	19.6162	19.5172
	70	18.5627	18.6785	18.9245	19.1076

Bold indicates straight fiber layups with equal starting and ending angles.

TABLE 12 The first two natural frequencies of the VSCL sandwich square plate $[(\Theta_0|\Theta_1)/core/(\Theta_0|\Theta_1)]$, CFCF.

Mode	Θ_0	Θ_1			
		0	30	50	70
1	0	25.3726	25.8954	27.2084	29.2269
	30	25.7569	26.5778	27.5736	29.7863
	50	26.7126	27.1244	28.5534	29.9713
	70	28.5698	28.9347	29.5431	30.5653
2	0	31.2536	31.9102	33.0809	34.7477
	30	31.8534	33.8788	34.1746	34.3478
	50	32.4782	34.2378	34.3559	34.6023
	70	33.4789	34.2478	34.4823	34.6283

Bold indicates straight fiber layups with equal starting and ending angles.

$$\begin{aligned}
 w = \varphi_y = \frac{\partial \varphi_x}{x} = 0, \quad x = 0 \text{ or } x = 1, \\
 w = \varphi_x = \frac{\partial \varphi_y}{y} = 0, \quad y = 0 \text{ or } y = 1,
 \end{aligned}
 \tag{30}$$

(c) Free (F)

$$\begin{aligned}
 Q_x = M_x = M_{xy} = 0, \quad x = 0, \text{ or } x = 1, \\
 Q_x = M_y = M_{xy} = 0, \quad y = 0, \text{ or } y = 1,
 \end{aligned}
 \tag{31}$$

Substituting Equation 12 into Equation 31, gives the following Equation 32:

$$\begin{aligned}
 A_{45} \left(\varphi^y + \frac{\partial w}{\partial y} \right) + A_{55} \left(\varphi^x + \frac{\partial w}{\partial x} \right) &= 0, \\
 D_{11} \frac{\partial \varphi_x}{\partial x} + D_{12} \frac{\partial \varphi_y}{\partial y} + D_{16} \left(\frac{\partial \varphi_x}{\partial y} + \frac{\partial \varphi_y}{\partial x} \right) &= 0, \\
 D_{16} \frac{\partial \varphi_x}{\partial x} + D_{22} \frac{\partial \varphi_y}{\partial y} + D_{66} \left(\frac{\partial \varphi_x}{\partial y} + \frac{\partial \varphi_y}{\partial x} \right) &= 0, \quad x = 0 \text{ or } x = 1, \\
 A_{44} \left(\varphi_y + \frac{\partial w}{\partial y} \right) + A_{45} \left(\varphi_x + \frac{\partial w}{\partial x} \right) &= 0, \\
 D_{12} \frac{\partial \varphi_x}{\partial x} + D_{22} \frac{\partial \varphi_y}{\partial y} + D_{26} \left(\frac{\partial \varphi_x}{\partial y} + \frac{\partial \varphi_y}{\partial x} \right) &= 0, \\
 D_{16} \frac{\partial \varphi_x}{\partial x} + D_{22} \frac{\partial \varphi_y}{\partial y} + D_{66} \left(\frac{\partial \varphi_x}{\partial y} + \frac{\partial \varphi_y}{\partial x} \right) &= 0, \quad y = 0 \text{ or } y = 1,
 \end{aligned}
 \tag{32}$$

Equations 29–31 can be combined to express the boundary conditions for a sandwich plate with hybrid boundary conditions.

After applying the DQM to discretize the above equations, the following Equations 33–35 can be got.

(a) Clamped

$$\begin{aligned}
 W(\xi_1, \eta_j) = W(\xi_{N_x}, \eta_j) = W(\xi_i, \eta_1) = W(\xi_i, \eta_{N_y}) &= 0, \\
 \psi_x(\xi_1, \eta_j) = \psi_x(\xi_{N_x}, \eta_j) = \psi_x(\xi_i, \eta_1) = \psi_x(\xi_i, \eta_{N_y}) &= 0, \\
 \psi_y(\xi_1, \eta_j) = \psi_y(\xi_{N_x}, \eta_j) = \psi_y(\xi_i, \eta_1) = \psi_y(\xi_i, \eta_{N_y}) &= 0, \quad \xi = 0, 1 \text{ or } \eta = 0, 1
 \end{aligned}
 \tag{33}$$

TABLE 14 The first four natural frequencies of the VSCL and CSCL sandwich square plate $[\pm(\Theta_0|\Theta_1)/core/\pm(\Theta_0|\Theta_1)]$, CCCC.

Face sheets	$\pm<\Theta_0 \Theta_1>$	Mode			
		1	2	3	4
CSCL	$<0 0>$	39.6465	58.9464	65.5382	79.5688
	$\pm<10 10>$	39.7633	59.4381	65.2119	79.8171
	$\pm<20 20>$	40.2143	60.7233	64.8844	80.4201
	$\pm<30 30>$	40.7764	62.2097	64.6121	80.9608
	$\pm<40 40>$	41.1206	63.3955	64.1663	81.2667
	$\pm<50 50>$	41.1286	63.3893	64.1589	81.2711
	$\pm<60 60>$	40.7783	62.2134	64.6091	80.9550
	$\pm<70 70>$	40.2143	60.7233	64.8844	80.4201
	$\pm<80 80>$	39.7633	59.4381	65.2119	79.8171
	$\pm<90 90>$	39.6465	58.9464	65.5382	79.5688
VSCL	$<0 0>$	39.6465	58.9464	65.5382	79.5688
	$\pm<0 10>$	39.5995	59.0649	65.1865	79.4612
	$\pm<0 20>$	39.6158	59.4321	64.7485	79.4525
	$\pm<0 30>$	39.7611	59.9688	64.4655	79.6308
	$\pm<0 40>$	39.9594	60.5895	64.2308	79.8756
	$\pm<0 50>$	40.1837	61.2613	63.9596	80.1436
	$\pm<0 60>$	40.4192	62.0193	63.5153	80.4052
	$\pm<0 70>$	40.5387	62.6344	62.9034	80.5004
	$\pm<0 80>$	40.6371	62.9314	63.5687	80.6479
	$\pm<0 90>$	40.9426	63.2478	63.9742	80.9412

TABLE 15 The first four natural frequencies of the VSCL and CSCL sandwich square plate $[\pm(\Theta_0|\Theta_1)/core/\pm(\Theta_0|\Theta_1)]$, SSSS.

Face sheets	$\pm<\Theta_0 \Theta_1>$	Mode			
		1	2	3	4
CSCL	$<0 0>$	34.2107	54.0555	61.2997	74.7633
	$\pm<10 10>$	35.0924	55.0091	61.6123	75.6645
	$\pm<20 20>$	36.6785	56.8276	62.1063	77.1309
	$\pm<30 30>$	37.9304	58.8233	62.2413	78.1959
	$\pm<40 40>$	38.5861	60.7359	61.8691	78.8032
	$\pm<50 50>$	38.5955	60.7358	61.8698	78.8023
	$\pm<60 60>$	37.9282	58.8248	62.2369	78.1875
	$\pm<70 70>$	36.6879	56.8271	62.1069	77.1257
	$\pm<80 80>$	35.0924	55.0091	61.6123	75.6645
	$\pm<90 90>$	34.2107	54.0555	61.2997	74.7633
VSCL	$<0 0>$	34.2107	54.0555	61.2997	74.7633
	$\pm<0 10>$	34.6226	54.4466	61.4801	75.1274
	$\pm<0 20>$	35.4858	55.2652	61.8013	75.7836
	$\pm<0 30>$	36.3912	56.1253	62.0164	76.4088
	$\pm<0 40>$	37.1433	56.8983	62.0999	76.9914
	$\pm<0 50>$	37.7003	57.7874	61.9965	77.5991
	$\pm<0 60>$	38.0251	59.0446	61.4271	78.0214
	$\pm<0 70>$	37.8989	59.7674	60.3035	77.7714
	$\pm<0 80>$	38.3278	60.0235	60.7468	78.3712
	$\pm<0 90>$	38.7412	60.7456	60.9312	78.9178

(b) Simply supported

$$\begin{aligned}
 W(\xi_1, \eta_j) &= W(\xi_{N_x}, \eta_j) = 0, \\
 \psi_y(\xi_1, \eta_j) &= \psi_y(\xi_{N_x}, \eta_j) = 0, \\
 \sum_{m=1}^{N_x} A_{im} \psi_x(\xi_m, \eta_j) &= 0, \xi = 0, 1, \\
 W(\xi_i, \eta_1) &= W(\xi_i, \eta_{N_y}) = 0, \\
 \psi_x(\xi_i, \eta_1) &= \psi_x(\xi_i, \eta_{N_y}) = 0, \\
 \sum_{n=1}^{N_y} B_{jn} \psi_y(\xi_i, \eta_n) &= 0, \eta = 0, 1
 \end{aligned} \tag{34}$$

(c) Free

$$\begin{aligned}
 A_{45}(\xi_i) \left(\psi_{y,mn} + \sum_{n=1}^{N_y} \bar{B}_{jn}^{(1)} W_{in} \right) + A_{55}(\xi_i) \left(\psi_{x,mm} + \sum_{m=1}^{N_x} \bar{A}_{im}^{(1)} W_{mj} \right) &= 0, \\
 D_{11}(\xi_i) \sum_{m=1}^{N_x} \bar{A}_{im}^{(1)} \psi_{x,mj} + D_{12}(\xi_i) \sum_{n=1}^{N_y} \bar{B}_{jn}^{(1)} \psi_{y,in} + D_{16}(\xi_i) \left(\sum_{n=1}^{N_y} \bar{B}_{jn}^{(1)} \psi_{x,in} + \sum_{m=1}^{N_x} \bar{A}_{im}^{(1)} \psi_{y,mj} \right) &= 0, \\
 D_{16}(\xi_i) \sum_{m=1}^{N_x} \bar{A}_{im}^{(1)} \psi_{x,mj} + D_{26}(\xi_i) \sum_{n=1}^{N_y} \bar{B}_{jn}^{(1)} \psi_{y,in} + D_{66}(\xi_i) \left(\sum_{n=1}^{N_y} \bar{B}_{jn}^{(1)} \psi_{x,in} + \sum_{m=1}^{N_x} \bar{A}_{im}^{(1)} \psi_{y,mj} \right) &= 0, \\
 \xi = 0, \text{ or } \xi = 1, \\
 A_{44}(\xi_i) \left(\psi_{y,mn} + \sum_{n=1}^{N_y} \bar{B}_{jn}^{(1)} W_{in} \right) + A_{45}(\xi_i) \left(\psi_{x,mm} + \sum_{m=1}^{N_x} \bar{A}_{im}^{(1)} W_{mj} \right) &= 0, \\
 D_{12}(\xi_i) \sum_{m=1}^{N_x} \bar{A}_{im}^{(1)} \psi_{x,mj} + D_{22}(\xi_i) \sum_{n=1}^{N_y} \bar{B}_{jn}^{(1)} \psi_{y,in} + D_{26}(\xi_i) \left(\sum_{n=1}^{N_y} \bar{B}_{jn}^{(1)} \psi_{x,in} + \sum_{m=1}^{N_x} \bar{A}_{im}^{(1)} \psi_{y,mj} \right) &= 0, \\
 D_{16}(\xi_i) \sum_{m=1}^{N_x} \bar{A}_{im}^{(1)} \psi_{x,mj} + D_{26}(\xi_i) \sum_{n=1}^{N_y} \bar{B}_{jn}^{(1)} \psi_{y,in} + D_{66}(\xi_i) \left(\sum_{n=1}^{N_y} \bar{B}_{jn}^{(1)} \psi_{x,in} + \sum_{m=1}^{N_x} \bar{A}_{im}^{(1)} \psi_{y,mj} \right) &= 0, \\
 \eta = 0, \text{ or } \eta = 1,
 \end{aligned} \tag{35}$$

TABLE 16 The first four natural frequencies of the VSCL and CSCL sandwich square plate $[\pm(\Theta_0|\Theta_1)/core/\pm(\Theta_0|\Theta_1)]$, CSCS.

Face sheets	$\pm\langle\Theta_0 \Theta_1\rangle$	Mode			
		1	2	3	4
CSCL	$\langle 0 0\rangle$	37.5024	57.8947	62.3989	77.0217
	$\pm\langle 10 10\rangle$	37.8793	58.6101	62.5111	77.6454
	$\pm\langle 20 20\rangle$	38.6935	60.1009	62.6884	78.6969
	$\pm\langle 30 30\rangle$	39.4105	61.7087	62.6701	79.5307
	$\pm\langle 40 40\rangle$	39.6738	62.2541	63.0058	79.9913
	$\pm\langle 50 50\rangle$	39.4414	61.2449	63.7949	79.9937
	$\pm\langle 60 60\rangle$	38.8023	59.6105	64.2041	79.5934
	$\pm\langle 70 70\rangle$	37.8323	57.5893	64.3516	78.8537
	$\pm\langle 80 80\rangle$	37.5264	57.1583	64.1025	78.4527
	$\pm\langle 90 90\rangle$	37.2354	56.8524	63.9412	78.0278
VSCL	$\langle 0 0\rangle$	37.5024	57.8947	62.3989	77.0217
	$\pm\langle 0 10\rangle$	37.6643	58.1857	62.4688	77.2209
	$\pm\langle 0 20\rangle$	38.0344	58.8009	62.5795	77.6296
	$\pm\langle 0 30\rangle$	38.4568	59.4867	62.6558	78.0703
	$\pm\langle 0 40\rangle$	38.8543	60.1697	62.6324	78.5416
	$\pm\langle 0 50\rangle$	39.1992	60.9189	62.4429	79.0081
	$\pm\langle 0 60\rangle$	39.3641	61.7311	61.8114	79.2853
	$\pm\langle 0 70\rangle$	39.0592	60.2489	62.5273	79.1059
	$\pm\langle 0 80\rangle$	38.8257	59.5672	62.0147	78.8521
	$\pm\langle 0 90\rangle$	38.5178	59.1782	61.6871	78.2347

TABLE 17 The first four natural frequencies of the VSCL and CSCL sandwich square plate $[\pm(\Theta_0|\Theta_1)/core/\pm(\Theta_0|\Theta_1)]$, CFCF.

Face sheets	$\pm\langle\Theta_0 \Theta_1\rangle$	Mode			
		1	2	3	4
CSCL	$\langle 0 0\rangle$	25.3703	31.2492	49.9557	56.6619
	$\pm\langle 10 10\rangle$	25.5619	32.7302	50.2086	57.8003
	$\pm\langle 20 20\rangle$	26.2851	35.1405	51.1297	59.5543
	$\pm\langle 30 30\rangle$	27.5682	36.7949	52.8277	60.5013
	$\pm\langle 40 40\rangle$	28.8566	37.6394	54.8188	59.5414
	$\pm\langle 50 50\rangle$	29.7612	37.8786	56.4734	58.0694
	$\pm\langle 60 60\rangle$	30.3433	37.5588	56.1658	57.6965
	$\pm\langle 70 70\rangle$	25.3733	31.2523	49.9548	56.6652
	$\pm\langle 80 80\rangle$	25.1247	31.0247	49.2178	56.1247
	$\pm\langle 90 90\rangle$	25.0147	30.8563	48.3578	55.2357
VSCL	$\langle 0 0\rangle$	25.3703	31.2492	49.9557	56.6619
	$\pm\langle 0 10\rangle$	25.4315	31.5943	50.0411	56.9475
	$\pm\langle 0 20\rangle$	25.6361	32.3863	50.2951	57.6348
	$\pm\langle 0 30\rangle$	26.0476	33.3245	50.7796	58.5386
	$\pm\langle 0 40\rangle$	26.7302	34.2974	51.5551	59.6346
	$\pm\langle 0 50\rangle$	27.6357	35.2767	52.7227	60.9147
	$\pm\langle 0 60\rangle$	28.6174	36.2144	54.3692	60.8805
	$\pm\langle 0 70\rangle$	29.5493	36.8882	56.2009	59.7979
	$\pm\langle 0 80\rangle$	29.8971	37.2567	58.1478	60.8941
	$\pm\langle 0 90\rangle$	30.4526	37.8924	59.8654	61.7891

In this way, the specific matrix $\{T\}$ in Equation 26 can be calculated.

Figure 6 illustrates the solution procedure of the Differential Quadrature Method (DQM). The core concept involves replacing differential operations with a weighted summation of grid points (see Supplementary Appendix SI), significantly reducing computational dimensionality. By implementing the flowchart in MATLAB, the natural frequencies of sandwich plates can be effectively determined.

3 Results and discussion

3.1 Validation and convergence studies

The validation and convergence investigations of the free vibration for VSCL sandwich plates using the DQM solution method

are provided in this part. By comparing the results with other FSDT-based numerical solution solutions for currently available CSCL sandwich plates, the quantity of DQM grid points was ascertained.

Since the skins of a sandwich structure provides the main load-carrying capacity, the core transfers the load between the skins. Therefore, in terms of material selection, skins are usually made of high-strength and lightweight materials, while the core is selected as a flexible layer with low density and good energy absorption capability. In the selection of skins and cores for aircraft and spacecraft, aluminum alloys, carbon fibers, and glass fibers are usually chosen as skin materials, while the core can be made of solid low-density materials, honeycomb-like expanded high-density materials, and corrugated expanded high-density materials. Based on the above requirements, the Mechanical properties of the materials selected for this work are listed in Table 1. In the study,

TABLE 18 The first four natural frequencies of the VSCL and CSCL sandwich square plate $[\pm(\theta_0|\theta_1)/\text{core}/\pm(\theta_0|\theta_1)]$, CFFF.

Face sheets	$\pm\langle\theta_0 \theta_1\rangle$	Mode			
		1	2	3	4
CSCL	$\langle 0 0\rangle$	8.5282	16.5998	27.9785	30.2843
	$\pm\langle 10 10\rangle$	8.6335	18.0326	28.2266	31.9156
	$\pm\langle 20 20\rangle$	9.0336	20.3567	29.0842	35.0327
	$\pm\langle 30 30\rangle$	9.8914	21.9399	30.6438	39.7197
	$\pm\langle 40 40\rangle$	11.1856	22.6782	32.7076	47.1182
	$\pm\langle 50 50\rangle$	12.6164	22.7131	35.0052	47.6474
	$\pm\langle 60 60\rangle$	13.8076	22.0365	37.2562	44.5822
	$\pm\langle 70 70\rangle$	14.5736	20.6705	38.9595	41.8909
	$\pm\langle 80 80\rangle$	15.4788	22.6871	39.4871	47.8712
	$\pm\langle 90 90\rangle$	16.2357	23.9745	40.8912	48.6812
VSCL	$\langle 0 0\rangle$	8.5282	16.5998	27.9785	30.2843
	$\pm\langle 0 10\rangle$	8.5626	16.8994	28.0598	30.7746
	$\pm\langle 0 20\rangle$	8.6754	17.5511	28.3184	32.1932
	$\pm\langle 0 30\rangle$	8.9182	18.3178	28.8461	34.7479
	$\pm\langle 0 40\rangle$	9.3943	19.0856	29.7155	39.1078
	$\pm\langle 0 50\rangle$	10.2252	19.8431	31.0342	44.8934
	$\pm\langle 0 60\rangle$	11.4782	20.5674	32.9513	46.3146
	$\pm\langle 0 70\rangle$	12.9179	21.1012	35.5303	35.5345
	$\pm\langle 0 80\rangle$	13.6567	22.5481	36.7841	46.7812
	$\pm\langle 0 90\rangle$	14.8455	23.4841	37.5984	48.6944

material I and material III in Table 1 were used as the skins and the core, respectively.

First, the quantity of grid points at which the natural frequency generated by this method might be stabilized is determined by selecting an anti-symmetric sandwich plate of $[0/90/\text{core}/0/90]$ with the geometric parameters $a/b = 0.5$, $a/h = 10$, and $t_c = t_f = 10$. With an increasing number of grid points, Figure 7 displays the pattern of the sandwich plate's first three orders of natural frequency. It is evident that when the quantity of grid points rises, the frequency values' computation results typically yield steady results. It shows that the application of DQM to the problem in this study can provide convergent results.

The quantity of grid points in this investigation was selected as $N_x = N_y = 19$ when DQM was used. For comparison, various aspect ratios (a/h) and (a/b) were chosen, as shown in Tables 2, 3.

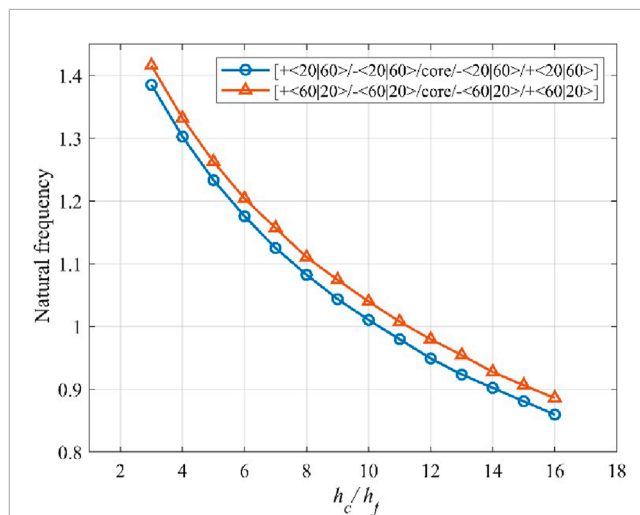


FIGURE 8 Natural frequency (non-dimensional) to core/skin ratio h_c/h_s effect of the symmetric VSCL sandwich plate $[+\langle 20|60\rangle/-\langle 20|60\rangle/\text{core}/-\langle 20|60\rangle/+\langle 20|60\rangle]$ and $[+\langle 60|20\rangle/-\langle 60|20\rangle/\text{core}/-\langle 60|20\rangle/+\langle 60|20\rangle]$, CSCS.

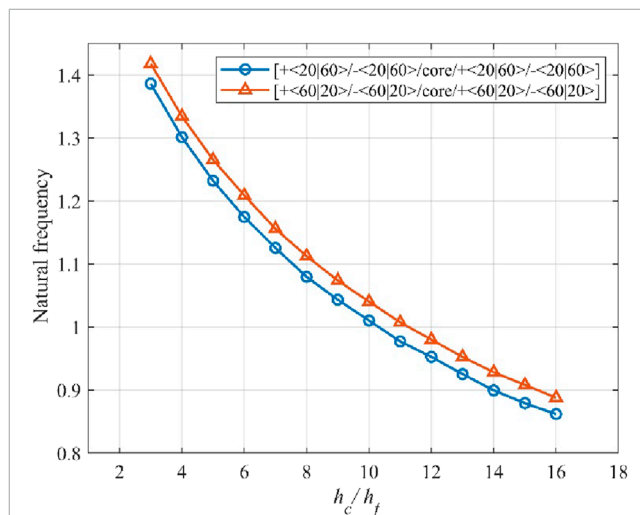


FIGURE 9 Natural frequency (non-dimensional) to core/skin ratio h_c/h_s effect of the anti-symmetric VSCL sandwich plate $[+\langle 20|60\rangle/-\langle 20|60\rangle/\text{core}/+\langle 20|60\rangle/-\langle 20|60\rangle]$ and $[+\langle 60|20\rangle/-\langle 60|20\rangle/\text{core}/+\langle 60|20\rangle/-\langle 60|20\rangle]$, CSCS.

As is evident from Tables 2 and 3, the results of the DQM used in this study to calculate the composite sandwich plates are only slightly different from those of the references, indicating that the mechanical model and calculation method used in this study are correct. At the same time, only 19×19 grid points are used in this study, which enables high accuracy of the results. Regarding computation effectiveness, the current paper's approach is better.

The free vibration analysis of VSCL plate is carried out in the next step. The first four orders of the natural frequency of the single layer plate are investigated for different starting angle θ_0 and termination angle θ_1 . The first four orders of the natural frequency of the

single layer plate are investigated. Different boundary conditions are selected. The material was chosen as material II in Table 1 and the ratio of width to thickness a/h was chosen as 0.001. The results of the calculations are listed in Table 4. When the number of mesh points was selected as 19, the computed results were compared with the existing solutions of FSDT and p -version finite elements. The computational results are in very good agreement, verifying the reliability of the present method for VSCL plate computation.

3.2 Parameter study

A parameter research of the free vibrations was carried out to enhance the vibratory behavior of the VSCL sandwich plates. The fundamental frequency of the sandwich plate was examined in relation to the fiber orientation angles, boundary conditions, number of layers, and core/skin thickness.

3.3 Fiber orientation angles

First, the effect of changes in the start and termination angles was investigated. In this section, a VSCL sandwich plate with four symmetric skins $[\pm(\Theta_0|\Theta_1)_s/core/\pm(\Theta_0|\Theta_1)_s]$ is chosen as the object of investigation. Materials II in Table 1 were used as the face sheets and materials IV and VI in Table 1 were used as the two kinds of core, respectively. Among the two selected core materials, material VI is an aluminum honeycomb core. (Torabi et al., 2019). The plate thickness $h = 0.1a$, the core thickness $h_c = \frac{4h}{5}$, and each single layer were taken as $h_{layer} = \frac{h}{40}$. For comparison, the first and second dimensionless natural frequencies $\bar{\omega} = \frac{\omega b^2}{h} \sqrt{\left(\frac{\rho}{E_2}\right)_f}$ were chosen. The fiber orientation angles Θ_0 and Θ_1 are both varied from 0° to 90° . Both CCCC and SSSS boundary conditions were considered, and the results are listed in Tables 5–8, respectively.

Tables 5–8 reveal that the majority of fundamental frequencies typically rise with the increase of fiber orientation angle. A corresponding decrease in the natural frequency was observed when the fiber orientation angle reached the maximum value. Therefore, sandwich plates can be made stiffer by using curvilinear fibers with low curvatures. In order to avoid fiber kinking, the curved fibers must have a maximum value of curvature on each skin of less than 3.28 m^{-1} . The curvature k is given by Equation 36. In the case of curved fibers with curvature values less than 3.28 m^{-1} , the use of lower curvature leads to higher stiffness. In certain instances, industry designers must alter the fundamental frequency to a greater or lesser value for the purpose of preventing resonance. This can be accomplished by using VSCL, sandwich plates without having to change the size of the plate or constituent materials. The reason for this is that the natural frequency is sensitive to changes in fiber orientation in each layer.

$$k = \frac{2}{a}(\Theta_1 - \Theta_0) \cos \left[\Theta_0 + \frac{2}{a}(\Theta_1 - \Theta_0)x \right] \quad (36)$$

3.4 Boundary conditions

In order to investigate the first two fundamental frequencies at various fiber orientation angles, five boundary conditions were taken

into consideration in this section. A comparative study between the CSCL and VSCL sandwich plates was also conducted. In this section, sandwich plates with single-ply skins $[\langle\Theta_0|\Theta_1\rangle/core/\langle\Theta_0|\Theta_1\rangle]$ are chosen, and the fiber orientation angles Θ_0 and Θ_1 are varied from 0° to 70° . Materials II and V from Table 1 were used as the skins and the core, respectively. The plate thickness $h = 0.1a$, core thickness $h_c = \frac{8h}{9}$, and each single layer were taken as $h_{layer} = \frac{h}{18}$. Tables 9–13 present the results with five boundary conditions: CCCC, SSSS, CSCS, CFCF, and CFFF. The natural frequencies of the CSCL sandwich plates are bolded in these tables.

Tables 9–13 demonstrate that for the SSSS, CSCS, CFCF, and CFFF boundary conditions, the VSCL sandwich plate's natural frequency tends to grow when the ending angle Θ_1 increases, the situation is reversed for the CCCC. For CFCF and CFFF, the VSCL sandwich plate's fundamental frequency increased by 15.175% and 32.708%, respectively, when the ending angle Θ_1 was increased from 0° to 70° . Nonetheless, under SSSS and CSCS boundary circumstances, the VSCL sandwich plate's fundamental frequency dropped by 2.228% and 1.128%, respectively, when the endings angle Θ_1 is increased from 50° to 70° . The VSCL plate fundamental frequency (non-bolded data) is improved by up to 9.7% at the CCCC boundary. The present method requires only $19^2 = 361$ grid points, which is 83% less computationally time-consuming than Hachemi's (Hachemi et al., 2020) p -type finite element (which typically requires >2000 nodes) (0.5 h vs 3 h). According to the findings, the fundamental frequencies of the VSCL sandwich plates are affected by the fiber orientation angle as the curvilinear fiber's curvature increases.

3.5 Limited layer impact (≤ 5)

This section looks into how the number of layers affects sandwich plate's fundamental frequency. Based on sandwich plates with single-ply skins $[\langle\Theta_0|\Theta_1\rangle/core/\langle\Theta_0|\Theta_1\rangle]$, the quantity of layers was increased, and sandwich plates with two-layer anti-symmetric skins $[\pm(\Theta_0|\Theta_1)/core/\pm(\Theta_0|\Theta_1)]$ were selected. The thicknesses and mechanical properties were selected to match those mentioned in the preceding section. The layup angle of VSCL and CSCL is set logically as follows: when $\Theta_0 = \Theta_1$, the curved fibers are degraded to straight fibers (i.e., VSCL = CSCL); and when $\Theta_0 \neq \Theta_1$, the VSCL achieves the performance gain through fiber path optimization. The CSCL data in the table are all for the degraded condition of $\Theta_0 = \Theta_1$, which is in direct comparison with the same angle VSCL. The results with five boundary conditions are listed in Tables 14–18.

From Tables 14–18, it is clear that when Θ_1 increases, the fundamental frequency shifts. In the CCCC boundary condition, when Θ_1 rises from 0° to 10° and from 10° to 90° , the natural frequency falls and increases, respectively. Under the SSSS and CSCS boundary conditions, the natural frequency increases when Θ_1 increases from 0° to 60° and decreases from 60° to 90° . When the number of layers increases, the fundamental frequency for sandwich plates with anti-symmetric two-layer skins often increases as well.

Under CCCC and CSCS boundary conditions, VSCL sandwich plates exhibit 6%–12% higher fundamental frequencies than CSCL counterparts. This was determined by comparing the fundamental frequencies of the two sandwich plates. Sandwich plate vibration properties can be considerably altered by the application of

curvilinear fiber. For instance, when comparing $\Theta_0 = \Theta_1 = 40^\circ$ to $\Theta_0 = \Theta_1 = 50^\circ$ under the boundary conditions of SSSS and CCCC, the fundamental frequency of CSCL plates is zero, but the fundamental frequencies of VSCL plates are changed when Θ_1 increases from 40° to 50° .

3.6 Core/skin thickness

Sandwich plates that are symmetric and anti-symmetric are used in this part to investigate the relation between the fundamental frequency and the ratio of the core to skin. The skins and core were selected with the same thickness and mechanical characteristics as those in the preceding section, except for the plate thickness $h = 0.01a$. The core thickness/skin thickness, h_c/h_s , varied from 3 to 16 as variation parameters. The fundamental frequencies of $[\pm\langle\Theta_0|\Theta_1\rangle]_{core/\mp\langle\Theta_0|\Theta_1\rangle}$ and $[\pm\langle\Theta_0|\Theta_1\rangle]_{core/\pm\langle\Theta_0|\Theta_1\rangle}$ are chosen to study the variation rule and CSCS boundary condition is chosen. Changes in fundamental frequency with core/skin thickness ratio h_c/h_s are shown in Figures 8, 9.

As shown in Figures 8, 9, the VSCL sandwich plates exhibit the highest natural frequency at the lowest core/skin thickness ratio. The average decline in fundamental frequency from the greatest to the lowest point was 67%.

The findings of the aforementioned parametric study suggest that VSCL sandwich plates hold promise for aircraft panel design applications. By manipulating the starting and ending angles along with the curvature of the fiber reference path, these plates can potentially exhibit reduced lateral deformation, increased stiffness, and higher natural frequencies. Moreover, lower structural mass can be achieved under certain mechanical and environmental loading circumstances by using VSCL sandwich plates.

4 Conclusion

This study used FSDT in conjunction with DQM to examine the free vibration of sandwich plates with curvilinear fiber variable stiffness skins. In this study, the x -coordinate was supposed to fluctuate linearly with the fiber orientation angle. Compared with other numerical solution methods, the DQM is computationally inexpensive, converges quickly, and it is capable of precisely forecasting sandwich plate fundamental frequencies. The reduction or increase in the natural frequency when using VSCL face sheets was investigated and compared with that of CSCL face sheets. The impacts of fiber orientation angles, boundary conditions, number of layers, and core/skin thickness were investigated parametrically. Notably, the integration of higher-order theory and layer theory can enhance the accuracy of sandwich plate analysis, particularly when investigating thick plates. The computations used in this study allow for the following deductions.

- (1) In the vast majority of cases, as the fiber orientation angle increases, the fundamental frequency rises as well. Optimizing the curved fiber path improves the fundamental frequency of the CFFF boundary condition by 32.7% and the CFCF boundary condition by 15.2%, outperforming the constant stiffness design (CSCL). The use of curvilinear fibers leads

to VSCL sandwich plates with lower lateral deformations and higher natural frequencies.

- (2) The sandwich plate's natural frequency was impacted by the fiber orientation angle as the curvilinear fibers' curvature grew. The larger the angle of the center fiber was, the more rigid the curvilinear fiber became, until the curvature threshold is reached (3.28 m^{-1}). The plate's rigidity can be raised by using low-curvature curvilinear fibers.
- (3) With an increase in layers came a rise in the sandwich plate's fundamental frequency. Anti-symmetric stacking ($\pm\langle\Theta_0|\Theta_1\rangle$) improves frequency by 6%–12% compared to single-layer skins. This also indicates that the fundamental frequency increases with rising plate thickness.
- (4) The VSCL sandwich plates exhibited greater natural frequencies in comparison to the CSCL sandwich plates when subjected to the CCCC and CSCS boundary conditions. As boundary restrictions get tighter, the frequency rises. Tighter boundaries (CCCC, CSCS) amplify the benefits of VSCL by more than 10%. Due to their increased ability to adapt to complex boundary circumstances, curvilinear fibers have higher fundamental frequencies than parallel fibers.
- (5) The frequency response was strongly impacted by the ratio of skin to core thickness. Frequencies peak at minimal h_c/h_s (3:1) and decline by 67% as ratios increase to 16:1. The natural frequency of the sandwich plate reached its maximum value at the lowest core-to-skin thickness ratio. The effect of adding more layers was in line with this trend.
- (6) The FSDT accuracy decreases for core-to-mask ratios $h_c/h_s > 16$ (see Table 2 for $a/h = 2$ error of 5.2%), and it is recommended that the HSDT model be used for thick plates.

The method proposed in this paper provides theoretical support for the vibration control design of lightweight structures in the aerospace field, such as enabling the adjustment of natural frequencies under specific operational conditions through fiber path optimization. Additionally, the precise insights obtained from this study guide researchers seeking viable solutions and can serve as a foundation for further exploration into panel flutter in VSCL sandwich plates. The current model does not consider interlayer delamination damage, and in the future, the Reissner interlayer continuity condition will be introduced to simulate the debonding effect and improve the damage tolerance prediction of VSCL sandwich plates.

Data availability statement

The original contributions presented in the study are included in the article/Supplementary Material, further inquiries can be directed to the corresponding author.

Author contributions

ZZ: Writing – review and editing, Software, Writing – original draft, Validation, Investigation, Conceptualization, Supervision, Methodology.

Funding

The author(s) declare that no financial support was received for the research and/or publication of this article.

Conflict of interest

The author declares that the research was conducted in the absence of any commercial or financial relationships that could be construed as a potential conflict of interest.

Generative AI statement

The author(s) declare that no Generative AI was used in the creation of this manuscript.

References

- Abrate, S. (2008). Functionally graded plates behave like homogeneous plates. *Compos. B. Eng.* 39, 151–158. doi:10.1016/j.compositesb.2007.02.026
- Akhavan, H., and Ribeiro, P. (2011). Natural modes of vibration of variable stiffness composite laminates with curvilinear fibers. *Compos. Struct.* 93, 3040–3047. doi:10.1016/j.compstruct.2011.04.027
- Akhavan, H., and Ribeiro, P. (2018). Aeroelasticity of composite plates with curvilinear fibers in supersonic flow. *Compos. Struct.* 194, 335–344. doi:10.1016/j.compstruct.2018.03.101
- Antunes, A. M., Ribeiro, P., Dias Rodrigues, J., and Akhavan, H. (2020). Modal analysis of a variable stiffness composite laminated plate with diverse boundary conditions: experiments and modelling. *Compos. Struct.* 239, 111974. doi:10.1016/j.compstruct.2020.111974
- Belarbi, M. O., Tati, A., Ounis, H., and Khechai, A. (2017). On the free vibration analysis of laminated composite and sandwich plates: a layerwise finite element formulation. *Lat. Am. J. Solids Struct.* 14, 2265–2290. doi:10.1590/1679-78253222
- Bellman, R., and Casti, J. (1971). Differential quadrature and long-term integration. *J. Math. Anal. Appl.* 34, 235–238. doi:10.1016/0022-247X(71)90110-7
- Birman, V., and Bert, C. W. (2002). On the choice of shear correction factor in sandwich structures. *J. Sandw. Struct. Mater.* 4, 83–95. doi:10.1177/1099636202004001180
- Carrera, E., and Brischetto, S. (2009). A survey with numerical assessment of classical and refined theories for the analysis of sandwich plates. *Appl. Mech. Rev.* 62, 1–17. doi:10.1115/1.3013824
- Civalek, Ö. (2008). Free vibration analysis of symmetrically laminated composite plates with first-order shear deformation theory (FSDT) by discrete singular convolution method. *Finite Elem. Anal. Des.* 44, 725–731. doi:10.1016/j.finel.2008.04.001
- Fu, T., Chen, Z., Yu, H., Wang, Z., and Liu, X. (2020). Free vibration of functionally graded sandwich plates based on nth-order shear deformation theory via differential quadrature method. *J. Sandw. Struct. Mater.* 22, 1660–1680. doi:10.1177/1099636218809451
- Ghandehari, M. A., Masoodi, A. R., and Hosseininia, E. S. (2025). Temperature-dependency and boundary condition impacts on the multiscale vibrational behavior of laminated nested dual conical shell structure semi-AUV applications. *Appl. Ocean. Res.* 154, 104425. doi:10.1016/j.apor.2025.104425
- Gürdal, Z., and Olmedo, R. (1993). In-plane response of laminates with spatially varying fiber orientations: variable stiffness concept. *AIAA J.* 31, 751–758. doi:10.2514/3.11613
- Hachemi, M. (2020). Vibration analysis of variable stiffness laminated composite sandwich plates. *Mech. Adv. Mater. Struct.* 27, 1687–1700. doi:10.1080/15376494.2018.1524951
- Hachemi, M. (2022). Layer-wise solutions for variable stiffness composite laminated sandwich plate using curvilinear fibers. *Mech. Adv. Mater. Struct.* 29, 5460–5477. doi:10.1080/15376494.2021.1956028
- Hachemi, M., Hamza-Cherif, S. M., and Houmat, A. (2020). Free vibration analysis of variable stiffness composite laminate plate with circular cutout. *Aust. J. Mech. Eng.* 18, 63–79. doi:10.1080/14484846.2017.1385694
- Houmat, A. (2020). Three-dimensional solutions for free vibration of variable stiffness laminated sandwich plates with curvilinear fibers. *J. Sandw. Struct. Mater.* 22, 896–925. doi:10.1177/1099636218778731
- Kant, T., and Swaminathan, K. (2001). Analytical solutions for free vibration of laminated composite and sandwich plates based on a higher-order refined theory. *Compos. Struct.* 53, 73–85. doi:10.1016/S0263-8223(00)00180-X
- Khani, A., Ijsselmuiden, S. T., Abdalla, M. M., and Gürdal, Z. (2011). Design of variable stiffness panels for maximum strength using lamination parameters. *Compos. Part B Eng.* 42, 546–552. doi:10.1016/j.compositesb.2010.11.005
- Langdon, G. S., von Klemperer, C. J., Rowland, B. K., and Nurick, G. N. (2012). The response of sandwich structures with composite face sheets and polymer foam cores to air-blast loading: preliminary experiments. *Eng. Struct.* 36, 104–112. doi:10.1016/j.engstruct.2011.11.023
- Liew, K. M., Han, J. B., Xiao, Z. M., and Du, H. (1996). Differential quadrature method for Mindlin plates on Winkler foundations. *Int. J. Mech. Sci.* 38, 405–421. doi:10.1016/0020-7403(95)00062-3
- Liew, K. M., Huang, Y. Q., and Reddy, J. N. (2003). Vibration analysis of symmetrically laminated plates based on FSDT using the moving least squares differential quadrature method. *Comput. Methods Appl. Mech. Eng.* 192, 2203–2222. doi:10.1016/S0045-7825(03)00238-X
- Liu, F. L. (2001). Differential quadrature element method for buckling analysis of rectangular mindlin plates having discontinuities. *Int. J. Solids Struct.* 38, 2305–2321. doi:10.1016/S0020-7683(00)00120-7
- Lopes, C. S., Gürdal, Z., and Camanho, P. P. (2008). Variable-stiffness composite panels: buckling and first-ply failure improvements over straight-fibre laminates. *Comput. Struct.* 86, 897–907. doi:10.1016/j.compstruc.2007.04.016
- Malikan, M., and Far, M. N. S. (2018). Differential Quadrature method for dynamic buckling of graphene sheet coupled by a viscoelastic medium using Neperian Frequency based on nonlocal elasticity theory. *J. Appl. Comput. Mech.* 4, 147–160. doi:10.22055/JACM.2017.22661.1138
- Mantari, J. L., and Ore, M. (2015). Free vibration of single and sandwich laminated composite plates by using a simplified FSDT. *Compos. Struct.* 132, 952–959. doi:10.1016/j.compstruct.2015.06.035
- Mindlin, R. D. (1951). Influence of rotatory inertia and shear on flexural motions of isotropic, elastic plates. *J. Appl. Mech.* 18, 31–38. doi:10.1115/1.4010217
- Mottaghi, T. H., Ghandehari, M. A., and Masoodi, A. R. (2025). Dynamic behavior of carbon nanotube-reinforced polymer composite ring-like structures: unraveling the effects of agglomeration, porosity, and elastic coupling. *Polym. (Basel)* 17, 696. doi:10.3390/polym17050696
- Noor, A. K., Burton, W. S., and Bert, C. W. (1996). Computational models for sandwich panels and shells. *Appl. Mech. Rev.* 49, 155–199. doi:10.1115/1.3101923
- Osa-uwagboe, N., Silberschmidt Vadim, V., Aremi, A., and Demirci, E. (2023). Mechanical behaviour of fabric-reinforced plastic sandwich structures: a state-of-the-art review. *J. Sandw. Struct. Mater.* 25, 591–622. doi:10.1177/10996362231170405
- Pandey, S., and Pradyumna, S. (2015). A new C0 higher-order layerwise finite element formulation for the analysis of laminated and sandwich plates. *Compos. Struct.* 131, 1–16. doi:10.1016/j.compstruct.2015.04.034

Publisher's note

All claims expressed in this article are solely those of the authors and do not necessarily represent those of their affiliated organizations, or those of the publisher, the editors and the reviewers. Any product that may be evaluated in this article, or claim that may be made by its manufacturer, is not guaranteed or endorsed by the publisher.

Supplementary material

The Supplementary Material for this article can be found online at: <https://www.frontiersin.org/articles/10.3389/fmats.2025.1601813/full#supplementary-material>

- Pany, C. (2022). An insight on the estimation of wave propagation constants in an orthogonal grid of a simple line-supported periodic plate using a finite element mathematical model. *Front. Mech. Eng.* 8, 1–13. doi:10.3389/fmech.2022.926559
- Pany, C., and Li, G. Q. (2023). Editorial: application of periodic structure theory with finite element approach. *Front. Mech. Eng.* 9, 2022–2024. doi:10.3389/fmech.2023.1192657
- Pushparaj, P., and Suresha, B. (2016). Free vibration analysis of laminated composite plates using finite element method. *Polym. Polym. Compos.* 24, 529–538. doi:10.1177/096739111602400712
- Reddy, J. N. (2004). *Mechanics of laminated composite plates and shells; theory and analysis*. Boca Raton, FL: CRC Press.
- Rezaiee-Pajand, M., and Masoodi, A. R. (2019). Shell instability analysis by using mixed interpolation. *J. Braz. Soc. Mech. Sci. Eng.* 41, 419–18. doi:10.1007/s40430-019-1937-y
- Setoodeh, S., Abdalla, M. M., Ijsselmuiden, S. T., and Gürdal, Z. (2009). Design of variable-stiffness composite panels for maximum buckling load. *Compos. Struct.* 87, 109–117. doi:10.1016/j.compstruct.2008.01.008
- Shu, C., Ding, H., and Yeo, K. S. (2004). Solution of partial differential equations by a global radial basis function-based differential quadrature method. *Eng. Anal. Bound. Elem.* 28, 1217–1226. doi:10.1016/j.enganabound.2003.02.001
- Shu, C., Yao, Q., Yeo, K. S., and Zhu, Y. D. (2002). Numerical analysis of flow and thermal fields in arbitrary eccentric annulus by differential quadrature method. *Heat Mass Transf. Stoffuebertragung* 38, 597–608. doi:10.1007/s002310100193
- Siriruk, A., Jack Weitsman, Y., and Penumadu, D. (2009). Polymeric foams and sandwich composites: material properties, environmental effects, and shear-lag modeling. *Compos. Sci. Technol.* 69, 814–820. doi:10.1016/j.compscitech.2008.02.034
- Thai, H.-T., Nguyen, T.-K., Vo, T. P., and Lee, J. (2014). Analysis of functionally graded sandwich plates using a new first-order shear deformation theory. *Eur. J. Mech. - A/Solids* 45, 211–225. doi:10.1016/j.euromechsol.2013.12.008
- Torabi, K., Afshari, H., and Aboutalebi, F. H. (2019). Vibration and flutter analyses of cantilever trapezoidal honeycomb sandwich plates. *J. Sandw. Struct. Mater.* 21, 2887–2920. doi:10.1177/1099636217728746
- Vinson, J. R. (1999). *The behavior of sandwich structures of isotropic and composite materials*. Lancaster, PA: Technomic.
- Vinson, J. R. (2001). Sandwich structures. *Appl. Mech. Rev.* 54, 201–214. doi:10.1115/1.3097295
- Whitney, J. M., and Pagano, N. J. (1970). Shear deformation in heterogeneous anisotropic plates. *J. Compos. Mater.* 37, 1031–1036. doi:10.1115/1.3408654
- Yaman, M., and Önal, T. (2016). Investigation of dynamic properties of natural material-based sandwich composites: experimental test and numerical simulation. *J. Sandw. Struct. Mater.* 18, 397–414. doi:10.1177/1099636215582216
- Yazdani, S., and Ribeiro, P. (2015). A layerwise p-version finite element formulation for free vibration analysis of thick composite laminates with curvilinear fibres. *Compos. Struct.* 120, 531–542. doi:10.1016/j.compstruct.2014.10.030
- Yuan, W. X., and Dawe, D. J. (2002). Free vibration of sandwich plates with laminated faces. *Int. J. Numer. Methods Eng.* 54, 195–217. doi:10.1002/nme.411
- Zare, M., Nazemzad, R., and Hosseini-Hashemi, S. (2015). Natural frequency analysis of functionally graded rectangular nanoplates with different boundary conditions via an analytical method. *Meccanica* 50, 2391–2408. doi:10.1007/s11012-015-0161-9